AD-A111 364 OHIO STATE UNIV COLUMBUS ELECTROSCIENCE LAB F/G 17/9
A SCATTERING MODEL FOR DETECTION OF TUNNELS USING VIDEO PULSE R--ETC(U)
FEB 77 L PETERS, G A BURRELL, H B TRAN DAAG53-76-C-0179
UNCLASSIFIED ESL-4460-3 NL

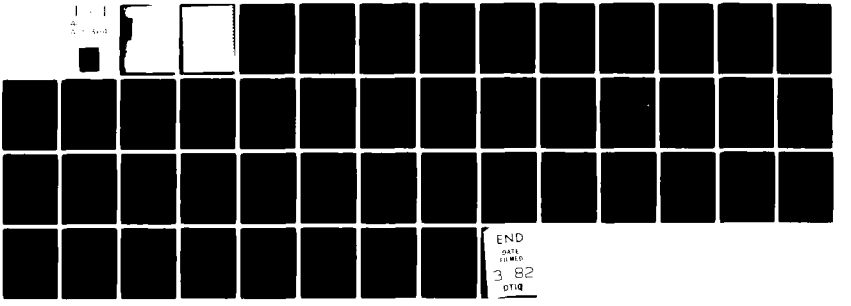

END
DATE FILMED
3 82
DTIC

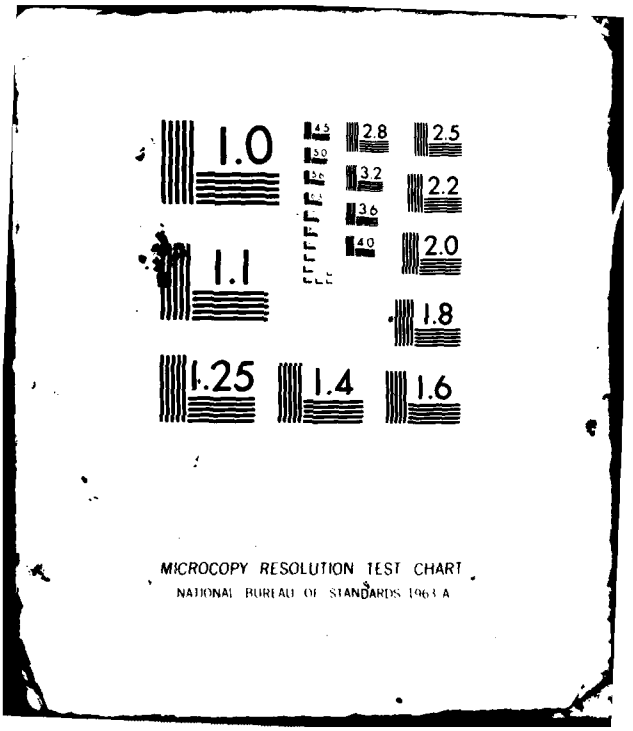
1.0
1.1
1.25
1.4
1.6
1.8
2.0
2.2
2.5
2.8
3.2
3.6
4.0
MICROCOPY RESOLUTION TEST CHART
NATIONAL BUREAU OF STANDARDS 1963 A

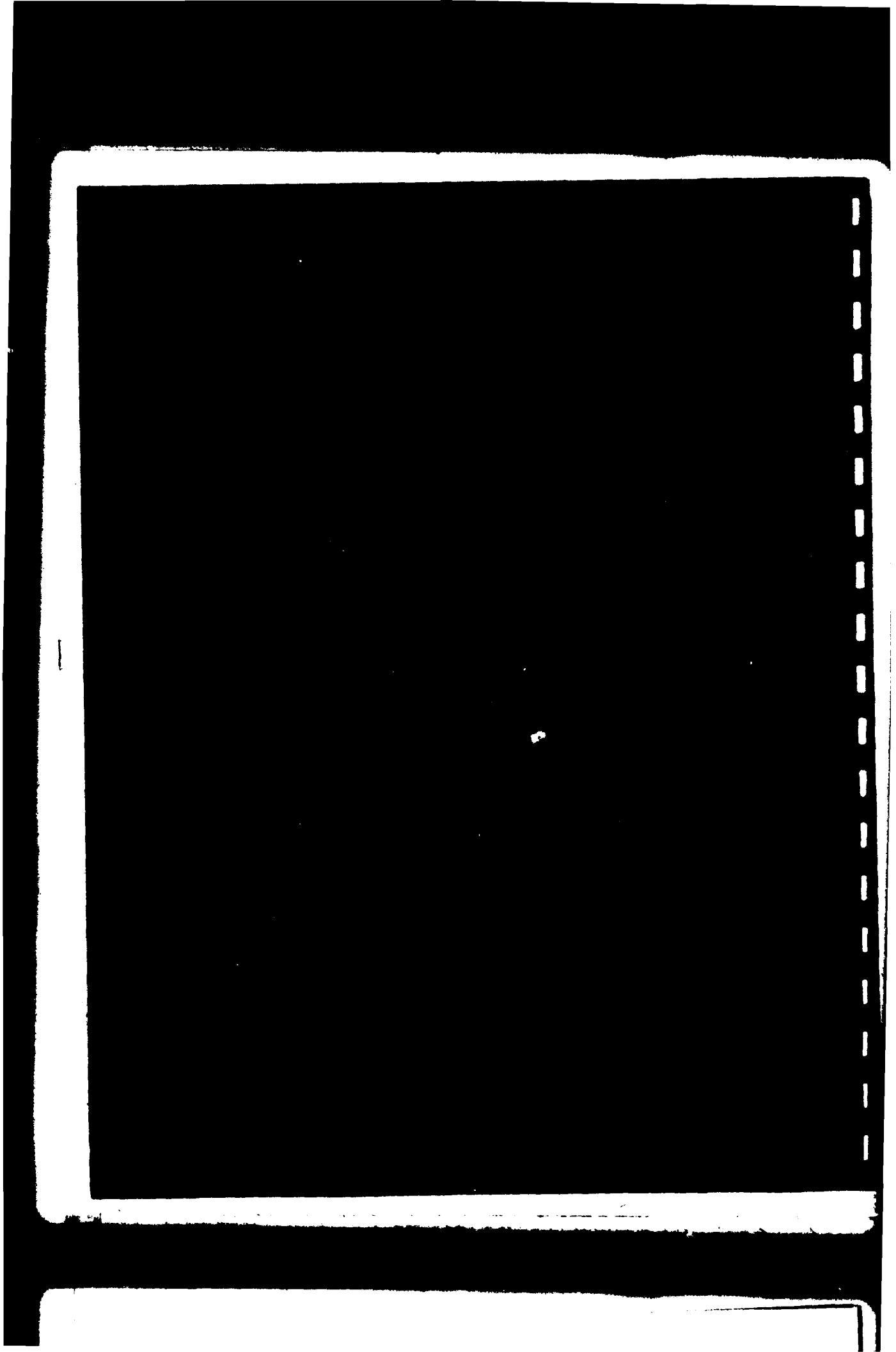

UNCLASSIFIED

SECURITY CLASSIFICATION OF THIS PAGE (When Data Entered)

REPORT DOCUMENTATION PAGE		READ INSTRUCTIONS BEFORE COMPLETING FORM
1. REPORT NUMBER	2. GOVT ACCESSION NO. AD-A114 364	3. RECIPIENT'S CATALOG NUMBER
4. TITLE (and Subtitle) A SCATTERING MODEL FOR DETECTION OF TUNNELS USING VIDEO PULSE RADAR SYSTEMS		5. TYPE OF REPORT & PERIOD COVERED Technical Report
		6. PERFORMING ORG. REPORT NUMBER ESL 4460-3
7. AUTHOR(s) L. Peters, Jr. G. A. Burrell H. B. Tran		8. CONTRACT OR GRANT NUMBER(s) Contract DAAG53-76-C-0179
9. PERFORMING ORGANIZATION NAME AND ADDRESS The Ohio State University ElectroScience Laboratory, Department of Electrical Engineering Columbus, Ohio 43212		10. PROGRAM ELEMENT, PROJECT, TASK AREA & WORK UNIT NUMBERS
11. CONTROLLING OFFICE NAME AND ADDRESS Department of the Army US Army Mobility Equipment Research & Development Command, Ft. Belvoir, Va 22060		12. REPORT DATE February 1977
		13. NUMBER OF PAGES 43
14. MONITORING AGENCY NAME & ADDRESS(if different from Controlling Office)		15. SECURITY CLASS. (of this report) Unclassified
		15a. DECLASSIFICATION/DOWNGRADING SCHEDULE

16. DISTRIBUTION STATEMENT (of this Report)

This document has been approved for public release and sale; its distribution is unlimited.

17. DISTRIBUTION STATEMENT (of the abstract entered in Block 20, if different from Report)

18. SUPPLEMENTARY NOTES

19. KEY WORDS (Continue on reverse side if necessary and identify by block number)

Tunnels
Electromagnetic Scattering
Conducting Media
Ground
Scattering Model
Infinite Circular Cylinder
Hollow Cylinders
Conducting Cylinders

20. ABSTRACT (Continue on reverse side if necessary and identify by block number)

Various cylindrical scattering models are used to outline the expected performance of video pulse radar systems for the detection of buried tunnels. A new scattering model is introduced which treats the tunnel scattering in terms of a Scattering Attenuation Function (SAF) separately from the transmission between dipole antennas in the earth, which is discussed in a previous report [9]. Examples of Scattering Attenuation Functions are

DD FORM 1 JAN 73 1473 EDITION OF 1 NOV 65 IS OBSOLETE

UNCLASSIFIED

SECURITY CLASSIFICATION OF THIS PAGE (When Data Entered)

20.

given for buried conducting cylinders, lossy cylinders, hollow cylinders (tunnels), and infinite tunnels containing conducting wires insulated from the surrounding earth. The features of these results and their influence on the choice of the radar parameters to detect the various geometries are discussed. Results are also presented for finite length tunnels containing conductors, and it is shown that the video pulse radar is inherently suitable for detecting such targets. Features of the results which would provide an identification capability are discussed.

TABLE OF CONTENTS

I. INTRODUCTION

The video pulse radar is now recognized as a viable tool for many applications, particularly for underground targets. Some of the more successful applications include the Terrascan pipe detection system [1,2], observation of geological targets [4,5,6], and archaelogical exploration [7]. In addition to pipes, many of the targets to be detected have a two dimensional nature, i.e., they can be modelled without significant error by an infinite cylinder of some shape. An example of this is a mine shaft. The presence of abandoned mine shafts leads to serious subsidence problems, and if these can be detected from the surface, then substantial loss of property could be avoided. Also many geological structures such as fault lines, some oil and gas traps can be represented as non circular cylindrical geometries. However, the antennas used to launch and receive an electromagnetic pulse to be used to detect such targets are finite in extent. For example, the antenna system used in the pipe detector video pulse radar is a pair of loaded crossed linear antenna elements as illustrated in schematic form in Figure 1. The transmit-receive (T-R) isolation is achieved by the orthogonal properties of the antenna. This orthogonal antenna system will respond to a linear target such as a thin wire that is responsive to only one linear polarization. It will also respond to any target which is located off the axis of symmetry of the antenna system. Obviously when the target is represented as an infinite cylinder, the antenna cannot be located in the far zone of the target. Therefore neither the echo width (W) concept for the infinite cylinder

$$W_e = \lim_{r\to\infty} 2\pi r \left| \frac{U_s}{U_i} \right|^2 \tag{1}$$

for two dimensional scatterers nor the echo area

$$A_e = \lim_{r\to\infty} 4\pi r^2 \left| \frac{U_s}{U_i} \right|^2 \tag{2}$$

for three dimensional scatterers are applicable.

A new model is introduced to obtain the voltage generated at the receiving antenna located at the same position in space as the transmitting antenna. Both receiving and transmitting antennas are finite length dipoles. This model treats separately the propagation phenomena between two dipoles separated twice the target distance in a homogeneous lossy media and the local scattering mechanisms, e.g., the infinite cylinder. The results are then combined to obtain the voltage generated at the terminals of the receiving antenna due to the scatterer.

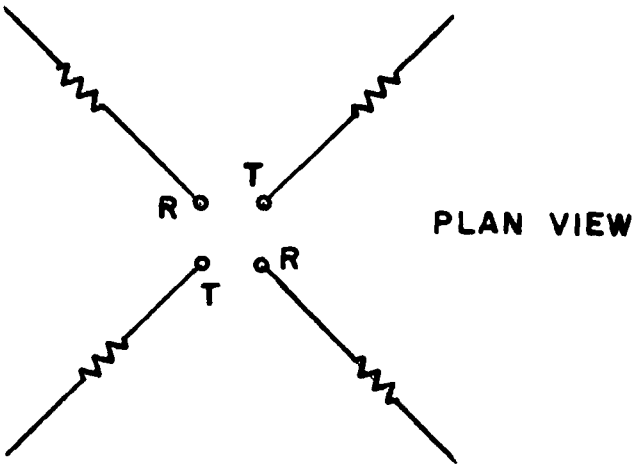

Figure 1. Diagramatic representation of orthogonal loaded dipole antenna system.

Alternatively the Green's function using an infinitesimal dipole at a finite distance from the cylinder could be invoked to obtain a solution for the scattered fields. A hybrid technique for the antenna currents which combines the moment method for the thin wire with the eigenfunction solution for the circular cylinder could be developed which would be applicable for circular cylinder. Such a solution has been recently developed by Wang and Richmond [8]. In general, the target is immersed in a lossy medium and the incident and reflected waves are attenuated as they propagate to and from the target. Thus, any of the conventional concepts for characterizing a scatterer would require a separate analysis for every target range, every antenna type and every set of electrical properties of the medium. Obviously, this leads to a prohibitively complex set of data to be obtained if a general underground radar system design is to be achieved.

In a previous report [9] we have discussed the means of obtaining the propagation of pulses between the transmit and receive antennas in a lossy media. The basic model is represented as the transmission between a pair of antennas immersed in the medium as is shown in Figure 2a. This transmission is represented in this report as V_R'/V_T where $2V_T$ is the Thevenin voltage of the generator driving the transmitting antenna and V_R' is the voltage generated across the load impedance attached to the receiving antenna. In this report we introduce the scattering from cylindrical targets into the model and calculate typical received signals.

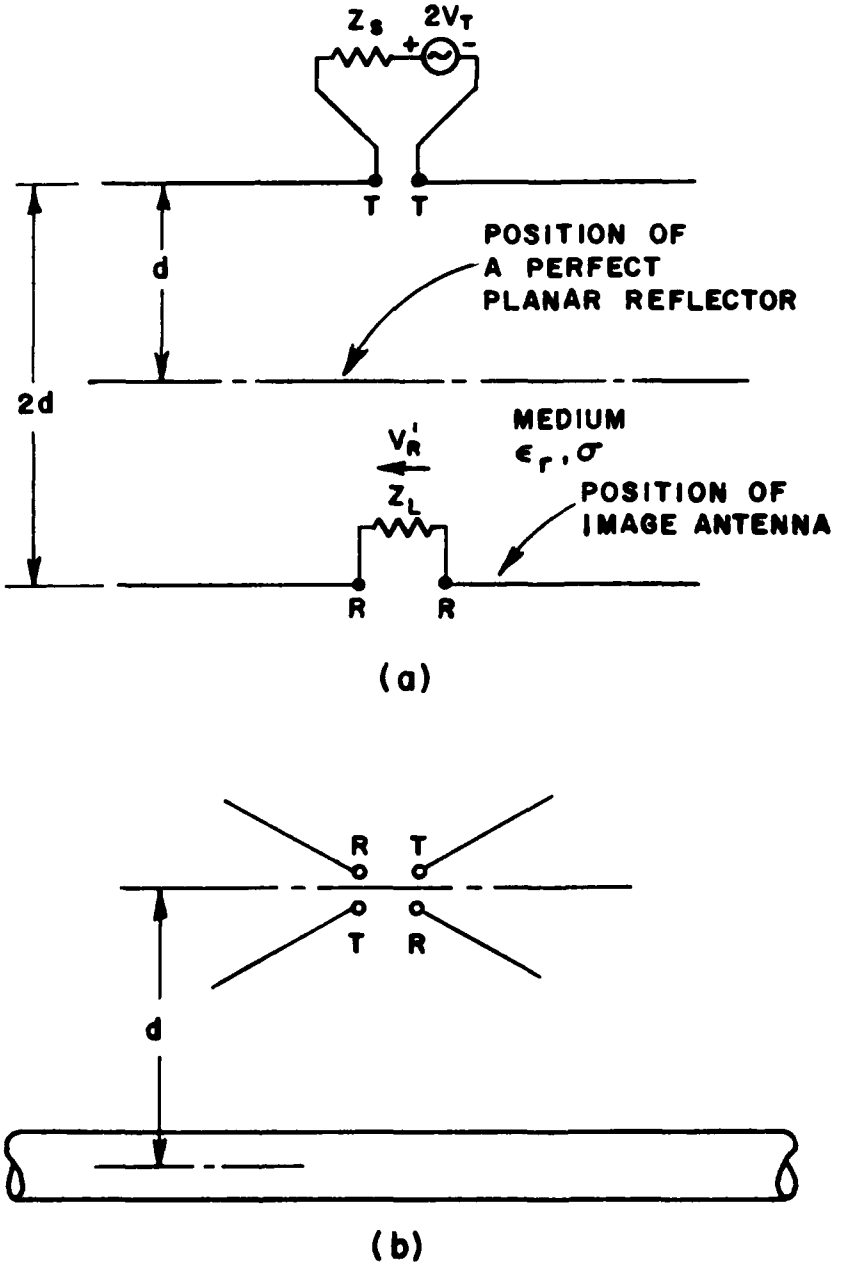

Figure 2. (a) Basic model for transmission between two antennas.
(b) Orthogonal dipole antenna system d meters from tunnel.

As discussed in a prior report [9], we have modelled the pulse generator by its Thevenin equivalent circuit. The Thevenin generator voltage is twice the output voltage, because in antenna engineering it is common to refer to the output voltage of a generator as the voltage delivered to a load whose impedance equals the generator source impedance. This voltage is V_T. In general the voltage appearing across the antenna terminals will not be V_T because the antenna impedance will vary with frequency. To obtain both the transmission and reflection characteristics of the pair of antennas in Figure 2(a) to the input pulse, the z-matrix of the two port network comprising the dipoles and the medium was computed for 512 equally spaced frequencies up to a maximum frequency which was about 2.5 times the highest frequency for which the input pulse had significant energy. The integral equation was solved for each frequency using a piecewise sinusoidal expansion for the current distribution [13]. From the z matrix data computed as a function of frequency, the signal reflected from the transmitting dipole and the signal generated across the load impedance terminating the receiving dipole can be computed [9].

II. SCATTERING MODELS

The ratio V_R'/V_T represents the relative terminal voltage obtained at the receiving antenna (across the load) for a perfect planar reflector at a depth d. If the scatterer is a simple planar lithologic contrast, this result would be modified by the reflection coefficient at the interface and the result would be exact. If the scatterer is a planar layer, the reflection coefficient of the layer would be used. If, in general, we define the Scattering Attenuation Function (SAF) as the modification of the scattered fields of the perfect planar reflector, then these reflection coefficients represent the SAF for these geometries. A curved interface such as a salt dome requires an additional correction factor.

A. Reflection from Convex Contrasts of Large Radii of Curvature

A geometrical optics approach [10,11] can be used to provide data for the scattered fields to a radar placed a distance d above a large curved surface to determine if such a discontinuity would be detectable from the surface. Geometrical optics is basically a high frequency concept. Energy propagates along a straight line path in a homogeneous medium; in our case, from the source to the target. At the target, these rays are scattered in the specular direction. The magnitude of the fields is obtained from the conservation of energy and after reflection these fields may be represented by a virtual source a distance ρ from the reflecting surface.

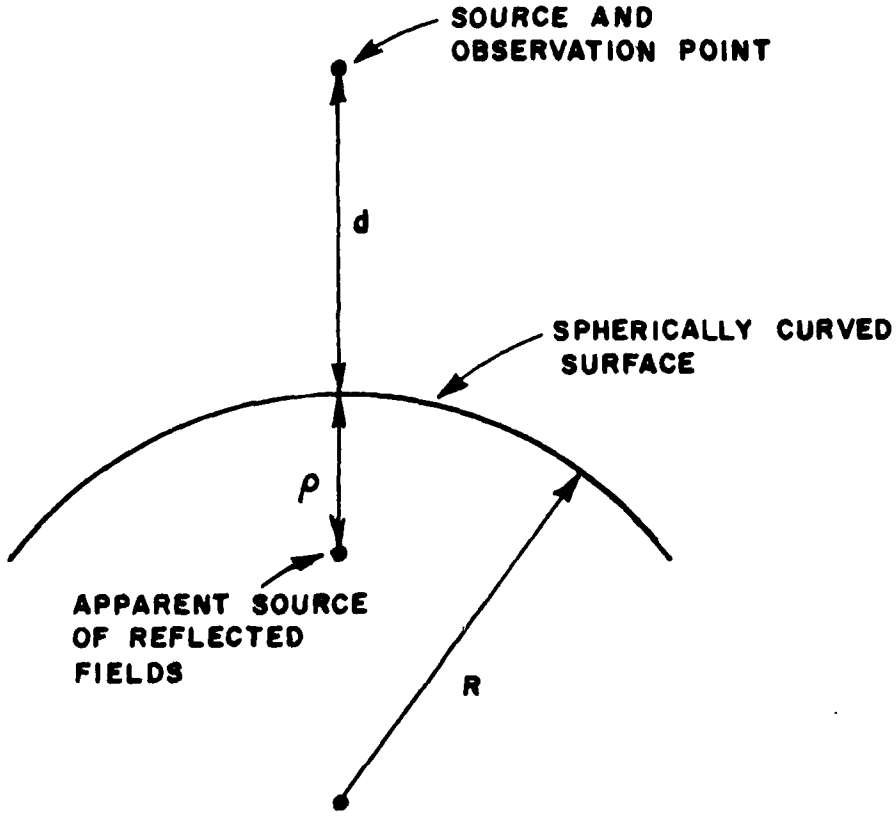

Figure 3. Depicting the apparent source of reflection from a spherically curved surface.

This assumes a spherical wave is launched by the probe from the feed terminals toward the spherical surface shown in Figure 3. This wave is reflected as though it were radiated by an apparent source a distance ρ below the curved surface where [10,11]

$$\rho = \frac{R\,d}{R + 2d} \qquad (3)$$

This gives rise to a scattered field at the radar

$$|U| = \frac{R}{2}\left[\frac{1}{R + d}\right] U_o\, e^{-2\gamma d} \tag{4}$$

where $U_o e^{-\gamma d}$ is the field incident at the curved surface. The attenuation and phase delay introduced by the lossy medium are displayed separately for convenience. Equation (4) reduces to the case of the planar interface discussed earlier as the radius R goes to infinity. The net loss introduced by the curvature is given by

$$\frac{U(R)}{U(R=\infty)} = \frac{R}{R + d} \quad . \tag{5}$$

We observe that when $R \approx d$, the scattered field is reduced by approximately a factor of two, and that when $R << d$, the scattered field reduction is of the order of R/d.

The reflecting surface need not be spherical and indeed can be represented by two principle radii of curvature R_1 and R_2. In this case, there are two virtual source positions, ρ_1, ρ_2 corresponding to the two principle radii of curvature. They are given by

$$\rho_i = \sqrt{\frac{R_i d}{R_i + 2d}} \tag{6}$$

These give rise to a reflected field of the form

$$|U| = \frac{1}{2}\sqrt{\frac{R_1}{R_1 + d} \cdot \frac{R_2}{R_2 + d}}\; U_o\, e^{-2\gamma d} \tag{7}$$

and a net loss of the form

$$\frac{U(R_1, R_2)}{U(R=\infty)} = \sqrt{\frac{R_1}{R_1 + d}\,\frac{R_2}{R_2 + d}} \quad . \tag{8}$$

The spherical "like" model of Figure 3 is not the only type of scatterer that may be of interest for geological exploration. Another possibility is that of a two dimensional or cylindrical (not necessarily circular) body. In this case, the apparent source position is different in the plane containing the axis of the cylinder and the plane orthogonal to it. This is represented by the general astigmatic ray

tube of geometrical optics. The apparent source position in the plane containing the axis of the cylinder is the same as was the case for scattering from the planar surface, i.e., $R_2 \to \infty$ in Equation (7).

The ratio given by Equation (7) now reduces to

$$\frac{U(R)}{U(R=\infty)} = \sqrt{\frac{R}{R+d}} \quad . \tag{9}$$

B. Model for Cylindrical Contrasts

The computation required for the singly curved or infinitely long cylindrical contrast does not require the use of geometrical optics and in fact can be obtained using any other method for computing the value of $U(R)/U(\infty)$. When the cylinder radius is small, the SAF can be computed conveniently by a modal solution [12] or by a moment method solution using polarization currents. Such a solution contains both the spatial divergence of the field reflected from the cylinder, the reflection coefficient introduced by a change in material at the interface, and the resonances which are characteristic of the cylinder. Figure 4 shows how we can obtain the radar return from an infinite cylinder using a scattering solution. First, we calculate the backscattered field E^S a distance d meters from the cylinder. This field is then related to the field which would be scattered by an infinite ground plane replacing the cylinder. Image theory is invoked, and as in Figure 4(b), we calculate the field E^I of an infinite line source 2d meters deep. E^S is now normalized by E^I to get the SAF(E^S/E^I), which is the representation of $U(R)/U(\infty)$.

From the model of the radar system with the perfectly reflecting interface [9], shown in Figure 4(c), we have obtained the medium loss, the antenna frequency response, and the spherical wave attenuation of the wave radiated by the dipole antenna. The effect of the cylinder is now simply introduced by multiplying the system response of the model by the SAF (E^S/E^I), i.e.,

$$V_T' = \frac{V_R'}{V_T} \frac{E^S}{E^I} \quad . \tag{10}$$

V_T' is now the received voltage on the terminals of the transmitting antenna due to the scatterer. This procedure is valid because the cylinder does not introduce additional wave divergence in the plane of the paper.

If the orthogonal antenna pair is used as shown in Figure 4(d), the voltage on the receiving antenna is

$$V_R = \frac{1}{2} \frac{V_R'}{V_T} \frac{E^S}{E^I} \quad . \tag{11}$$

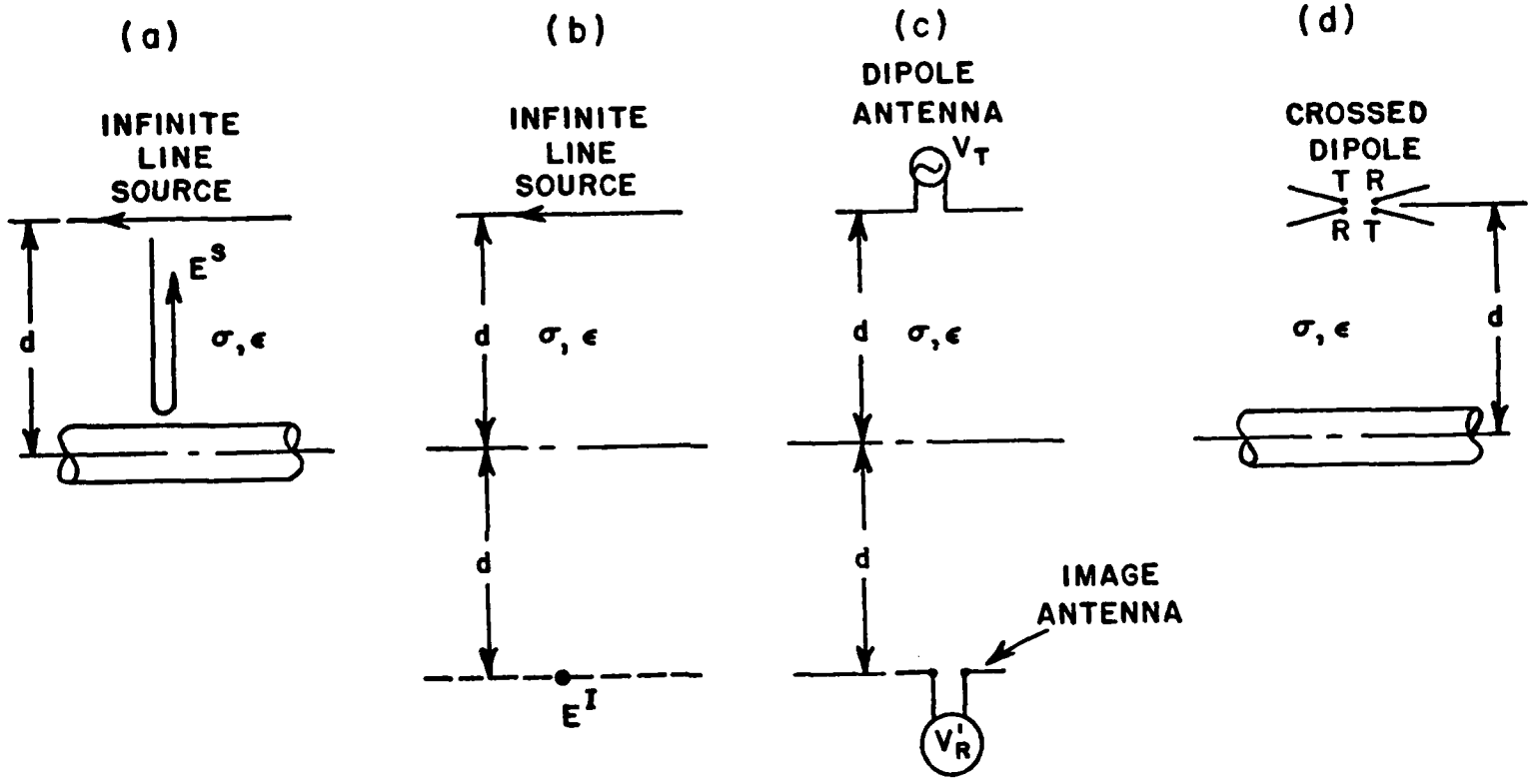

NORMALIZATION

$$\frac{E^S}{E^I}$$

$$\frac{V'_R}{V_T}$$

$$V_R = \frac{1}{2} \frac{V'_R}{V_T} \cdot \frac{E^S}{E^I}$$

Figure 4. Introducing the scattering attenuation function of a cylinder into the radar model.

The additional factor of 1/2 is introduced by the use of the crossed dipole geometry. This is introduced since the incident field component is oriented at 45° from the angle (0°) required for optimum excitation of the thin cylinder resulting in a 3 dB loss, and the receiving antenna is oriented at 45° to the scattered field resulting in another 3 dB loss. It is observed that these 3 dB factors depend on the linear target scattering being polarization dependent. This has led to much confusion for three dimensional targets and this will be discussed later in more detail. The major objective of this report is to introduce a model for the scattered field that extends this previous analysis to include the target scattering.

It may appear that this model is valid only for thin cylindrical contrasts primarily because the position of a reflecting plane is chosen to coincide with the position of the scatterer. For a tunnel sufficiently large that different scattering mechanisms can occur, such as those from the top and the bottom of the tunnel, then different reference planes could be required for the different scattering mechanisms in the same model. This would drastically increase the amount of data required for design and require a much more complex analysis. Fortunately as is shown in Appendix I, the choice of the position of this reflecting reference plane does not significantly influence the results and thus the technique should be reasonably valid for a thick cylindrical contrast.

C. A Check on the Validity of the Model for Thin Cylindrical Contrasts

The received voltage V_R of Figure 2(b) has been computed by a direct moment method solution to check the normalization procedure outlined in this report. For this comparison, an electrically small radius perfectly conducting circular cylinder was used because it could be analyzed by both methods. The moment method solution was by the sinusoidal reaction technique [13], so that the buried cylinder was required to be finite in length. The lossy medium attenuates the current on the cylinder as the distance from the excitation point becomes large so that the cylinder can be truncated without introducing significant error. We used a pair of 50 m long orthogonal dipoles 200 m from the center of a 1000 m long, 0.01 m radius wire. The antenna system was oriented for maximum signal (the plane of the antenna system was parallel to the plane containing the wire and the transmitting antenna was rotated 45° from the direction of the wire). The medium parameters were σ= 0.01 mhos/m and ϵ_r = 4. Figure 5 shows V_R when V_T is a 50 microsecond (μs) 1 volt gaussian input pulse [9] for both the moment method solution and the modal solution [12] modified in the way outlined above. The agreement in shape is almost exact and the amplitude difference of 0.8 dB (trivial considering the dynamic range of $\sim$140 dB) is attributed to the moment method solution because the cylinder was truncated. Note also that for the example a high conductivity was used, and the depth was 200 m, and yet this is a detectable pulse for a properly designed system.

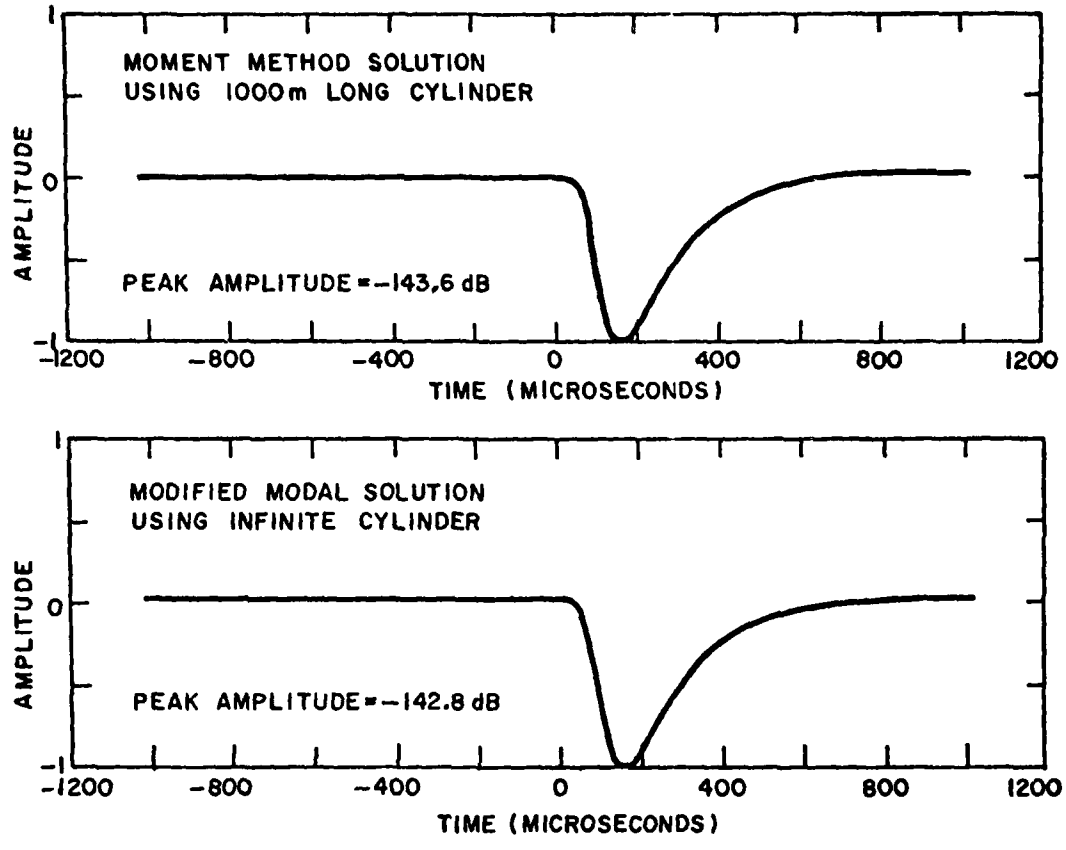

Figure 5. Comparison of received pulses obtained from complete moment method and modified modal solution. The antenna system was a pair of 50 m long orthogonal dipoles, and the target a 0.01 m radius wire 200 m from the antenna system. The constitutive parameters of the medium were σ=0.01 mhos/m, ε_r=4. The input pulse was a 50 μs gaussian.

III. SCATTERED FIELD PROPERTIES

There are a number of computer solutions now available for obtaining the scattered fields from infinite cylinders in a conducting medium when illuminated by a line source. Figure 6 shows the scattered fields normalized in the form E^S/E^I or H^S/H^I for 1 meter radius circular cylinders. Included in Figure 6 are curves for both perfectly conducting and hollow cylinders.

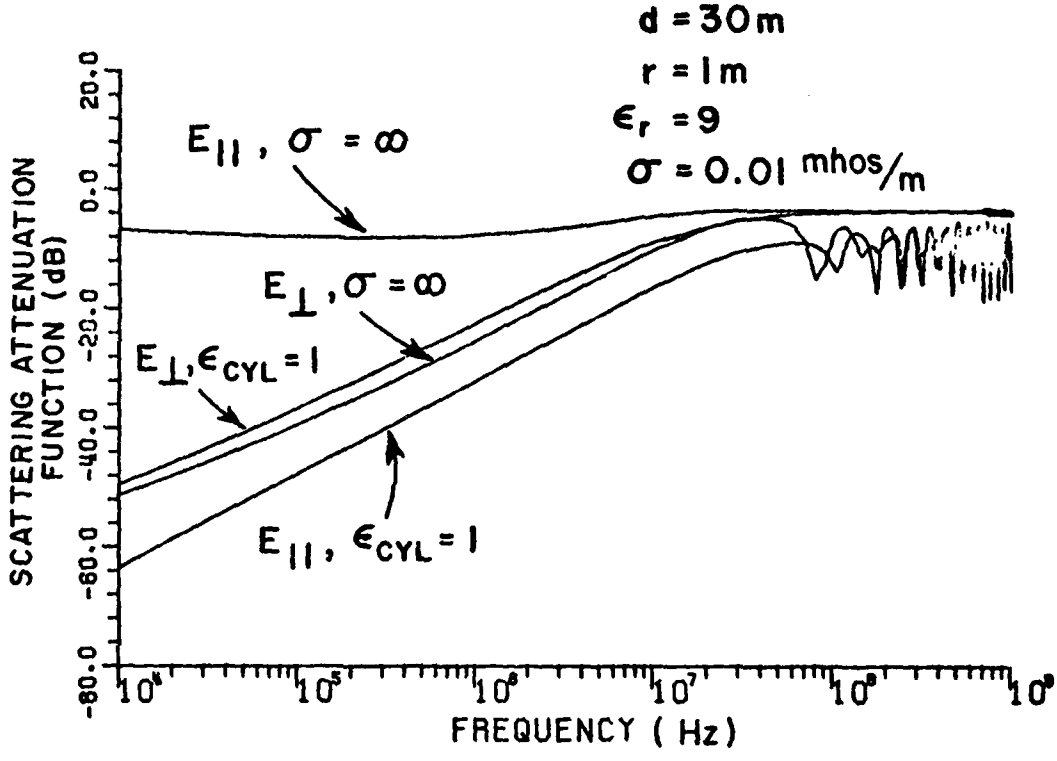

Figure 6. Scattering attenuation functions for a cylinder immersed in a ground like medium. Results are presented both for an air filled cylinder (ϵ_{CYL}=1) and a perfectly conducting cylinder (σ=∞).

The hollow or dielectric cylinders have been analyzed both by a modal solution and by a moment method solution commonly designated as the polarization current technique. The two solutions produce results within 0.01 dB for the circular cylinder, and the polarization current technique is being used to obtain E^S/E^I for non circular hollow cylinders. When the distance from the line source to the cylinder is large the scattered fields H^S/H^I can be taken to be the same as E^S/E^I since $E^S/E^I = ZH^S/ZH^I$ where Z is the intrinsic impedance of the media. H^S/H^I is designated $E_\perp$. E^S/E^I for polarization parallel to the cylinder is designated $E_{||}$.

A. Conducting Cylinders

For the conducting cylinder (which may be representative of a flooded tunnel) the normalized scattered field is almost frequency independent over a wide frequency range, and the reflected field is only about 5 dB less than that which would be obtained from a perfect reflecting plane. Consequently such a target would be very visible to a parallel polarized electromagnetic radar. If the radar is polarized perpendicular to the cylinder then the cylinder would be less visible to a radar operating at low frequencies than would the same cylinder oriented parallel to the radar antenna. Note that in Figure 6 no creeping wave resonances are observed in $E_{\perp}$ for the perfectly conducting cylinder. This is due to the lossy medium attenuating this wave. Figure 7 shows that this resonance is observed when the conductivity is reduced to σ = 0.0001 mhos/m.

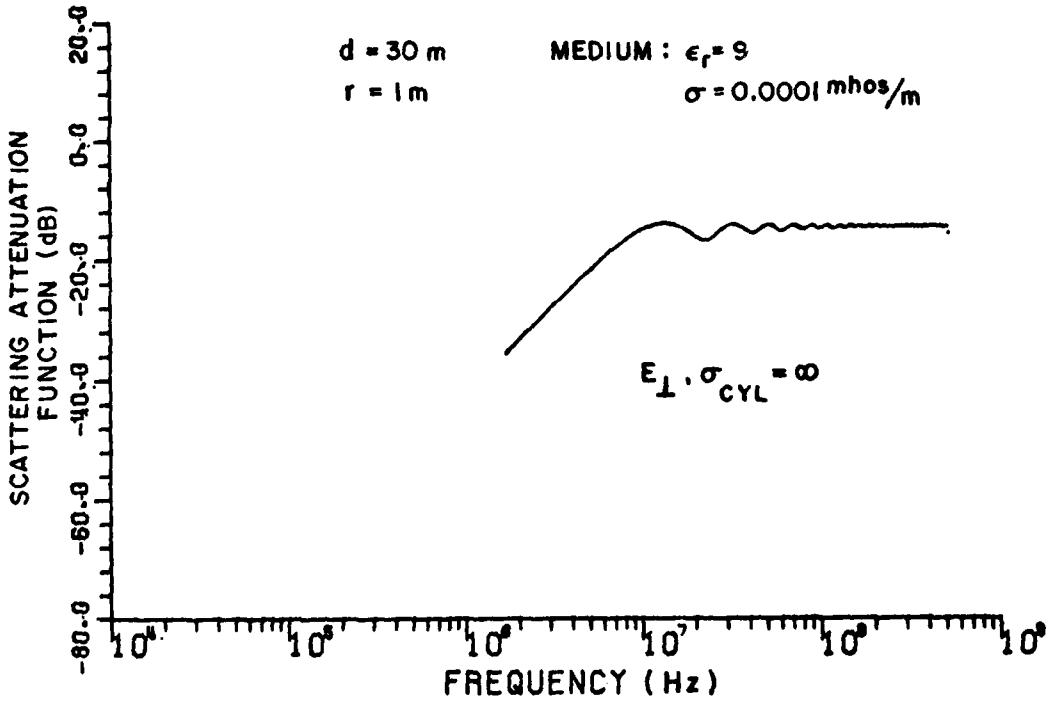

Figure 7. Scattering attenuation function for perfectly conducting cylinder and perpendicular polarization in relatively loss free ground.

The results for the conducting cylinder are similar to those which would be obtained for a flooded tunnel. Figure 8 shows the normalized scattered fields for lossy cylinders of varying conductivity. It is observed that the lossy cylinder behaves similarly to a conducting cylinder until the frequency decreases so that the tunnel diameter equals the skin depth. The conductivity of the water in a flooded tunnel could vary within wide limits, but would be of the order of 1 mho/m if significant quantities of mineral salts were dissolved.

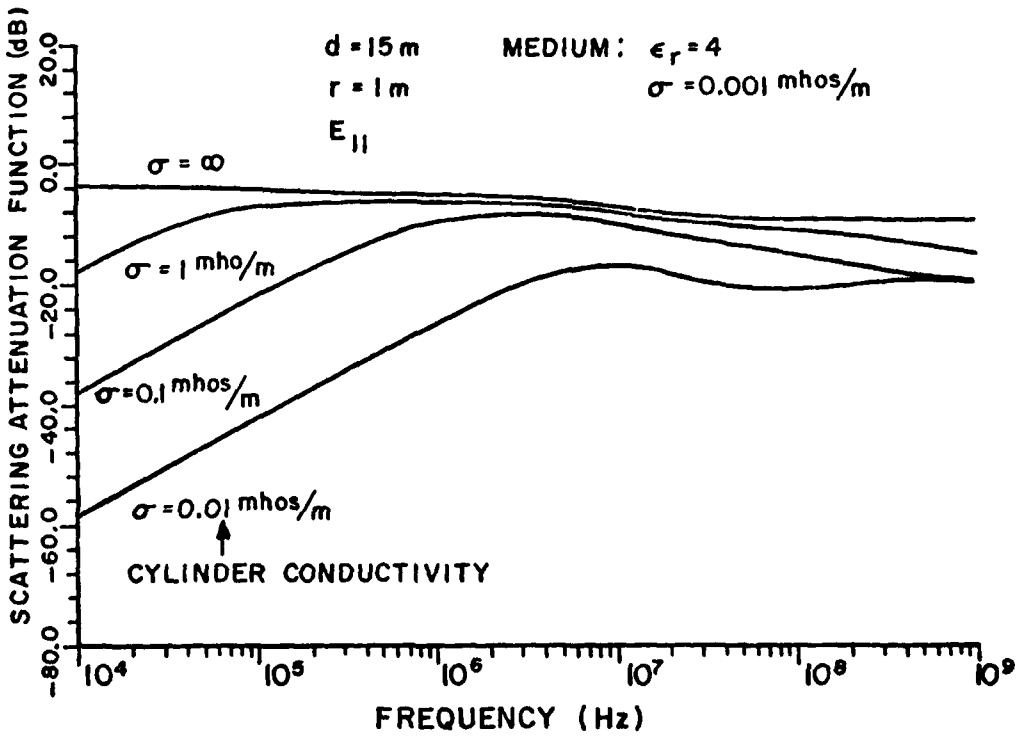

Figure 8. Scattering attenuation function for lossy dielectric cylinders in a lossy medium for parallel electric polarization.

B. Air Filled Circular Cylinders (Tunnels)

The scattered fields for the air filled infinite cylinders (tunnels) shown in Figure 6 are characterized by internal resonances. At frequencies higher than about the fourth resonance the scattered fields are the same for both polarizations: consequently at these frequencies the tunnel would not be detectable by electromagnetic means with an orthogonal antenna system. At frequencies lower than about the fourth resonance the fields scattered by the tunnel are different for the two polarizations.

Thus, in this frequency range, the tunnel is potentially detectable by an electromagnetic radar with an orthogonal antenna system. At low frequencies, when the tunnel is electrically small, the tunnel is 12-16 dB more visible to a perpendicularly polarized radar than it is to a parallel polarized radar. This is the reverse of the case of the conducting cylinder, and occurs because a transverse cylinder obstructs the current flow in the medium more than a parallel cylinder does.

For $E_{\parallel}$ the first resonance occurs when the tunnel diameter is approximately a half wavelength (a 1 m radius tunnel resonates at about 50 MHz). The resonances can be predicted quite accurately using Geometrical Optics [10]. For $E_{\parallel}$ only two rays need be considered for good engineering accuracy down to the first resonance [10]: These are the direct reflection from the tunnel roof and the ray which travels into the tunnel to be reflected from the tunnel floor. This simple representation, which is polarization independent, gives good accuracy above the fourth resonance for $E_{\perp}$. For $E_{\perp}$ below the fourth resonance, additional rays (which are polarization dependent) need to be included in the G.O. solution.

An important characteristic of the scattered fields of the air filled tunnels is that the resonance behavior is independent of depth and the electrical parameters of the ground. This first resonant region for 1 m radius tunnels lies between 40 MHz and 60 MHz. This has been verified for a range of:

conductivities	$.0001 \text{ mhos/m} \leq \sigma \leq 0.01 \text{ mhos/m}$,
permittivities	$4 \leq \varepsilon_r \leq 16$ and
depths	$15 \leq d < 120$ m.

Only the level of the curve changes significantly as these parameters are changed (additional curves are shown in Figure 9 for comparison). This remarkable behavior is a result of the fact that the resonances are caused by internal reflections. This is extremely important in terms of identification, i.e., a signal received by an electromagnetic radar operating in the resonance region will contain a signature of a hollow circular tunnel, and this signature will be relatively unaffected by the depth or the ground parameters. The only effect of the ground parameters on the shape of the curve in the resonant region is to alter the depth of the nulls: this occurs because a change in the Fresnel reflection coefficient alters the amplitudes of the direct reflection from the tunnel roof and the internal reflection from the tunnel floor. This effect can be observed in Figure 9.

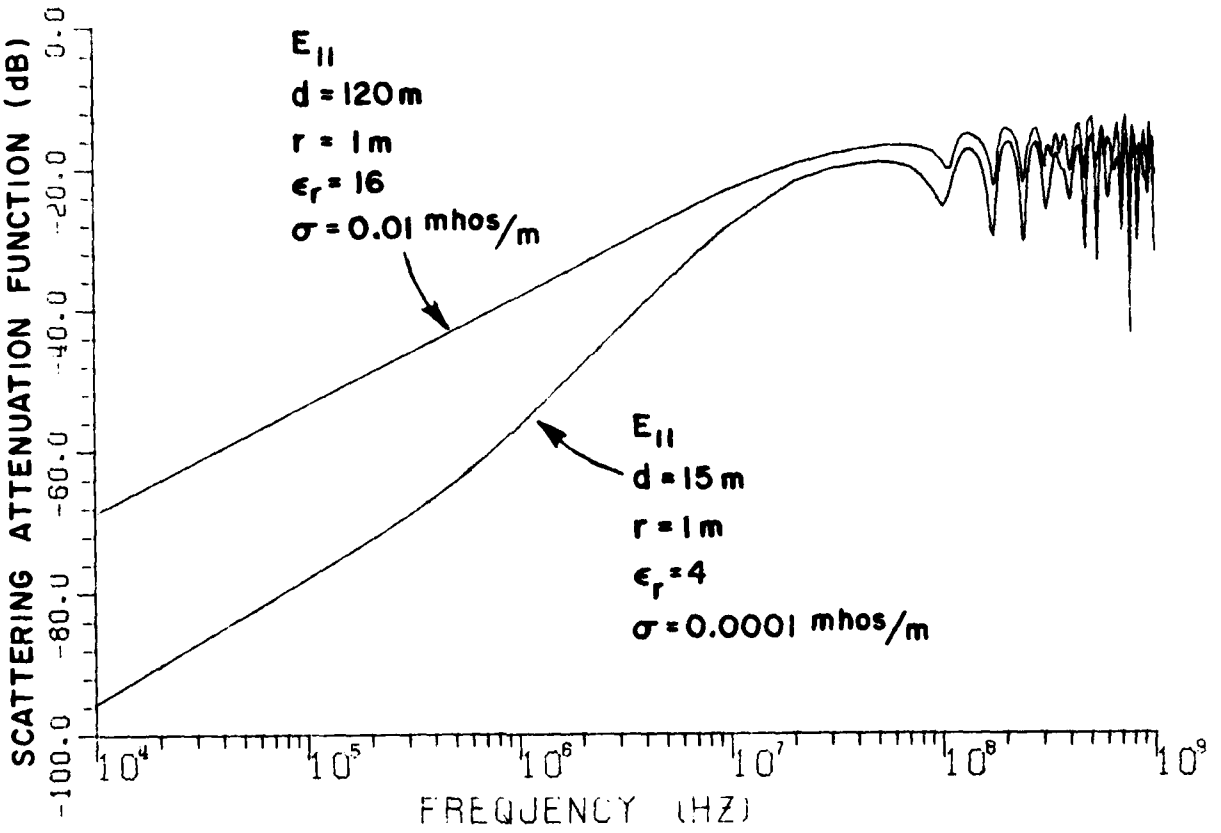

Figure 9. Comparison of scattering attenuation function for 1 m radius tunnel for different depths (d), dielectric constant (ϵ_r) and conductivity (σ) show that resonance region characteristics are insensitive to large variations in these parameters.

The level of the curve in the resonant region is affected by the value of the Fresnel reflection coefficient (which depends upon ϵ_r but not σ because at high frequencies the ground behaves like a lossy dielectric [9]) the depth and the attenuation constant of the medium. These affect the amplitude of of the curve in the following ways.

1) Increasing ϵ_r increases the value of the Fresnel reflection coefficient, so that the direct reflection from the top of the tunnel is increased, and the scattered field is increased.

2) Increasing σ (or decreasing ϵ_r) increases the attenuation constant α of the medium [9]. The scattered fields are normalized by the fields E^I scattered by a perfectly reflecting plane located at the axis of the cylinder, so that the E^I is lowered due to extra attenuation

introduced because the propagation distance involved is increased by twice the tunnel radius. Thus the normalized scattered fields E^S/E^I are increased. This effect can be very pronounced, as shown in Figure 10 where the conductivity is changed by an order of magnitude. The level change of 14.1 dB is exactly accounted for by the change in path loss over a distance equal to the radius of the cylinder.

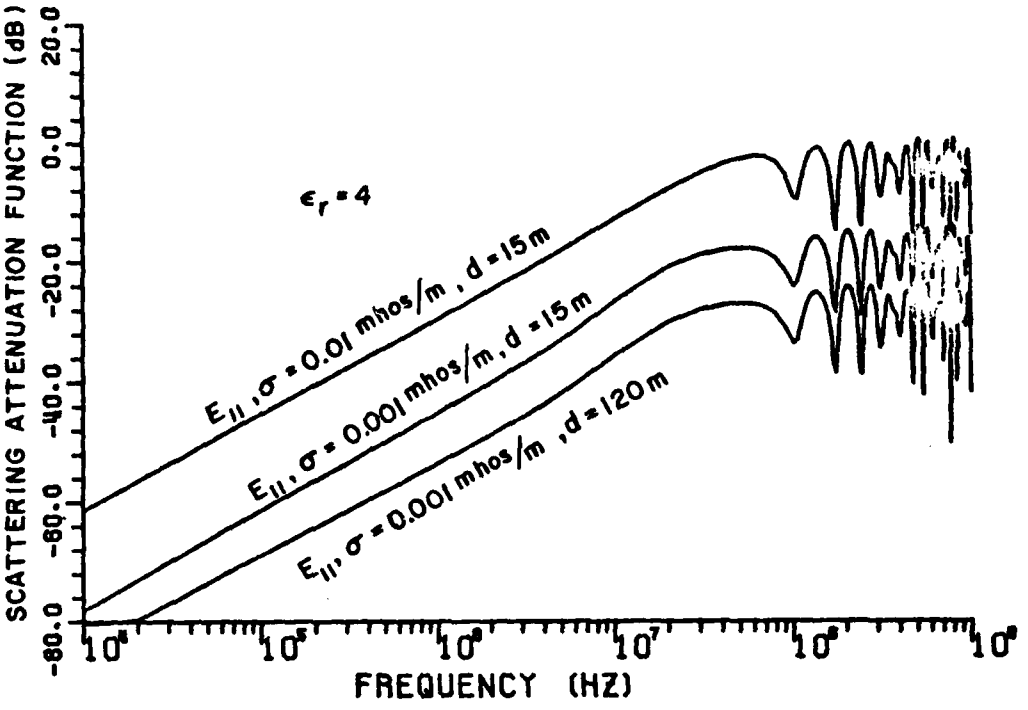

Figure 10. Comparison of scattering attenuation function for 1 m radius tunnel for different depths (d) and conductivity (σ) shows that the primary effect of these parameters is to change the amplitude of the curve.

3) As the depth is changed, the change in level of the curve is described by Equation (9). This is illustrated also in Figure 10 where a depth change from 15 m to 120 m results in an 8.79 dB change in level.

Figure 11 shows the scattered fields for a circular tunnel whose radius is two meters. This is, for all practical purposes, a frequency scaled version of the scattered fields for the 1 m radius tunnel. The segmented nature of this curve is due to insufficient data points.

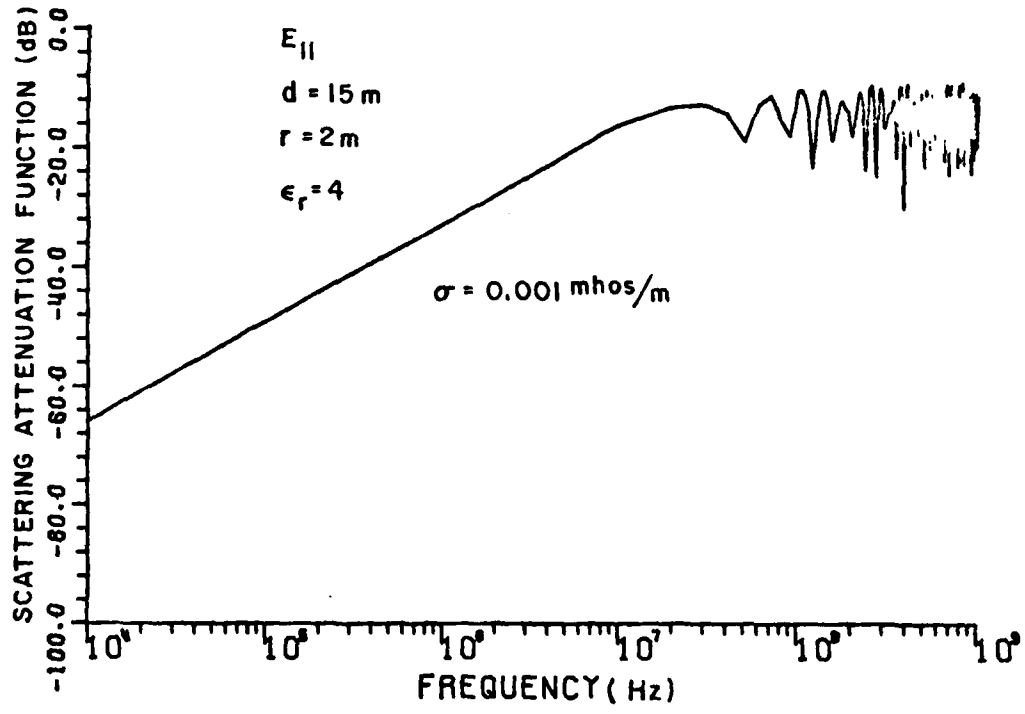

Figure 11. Scattering attenuation function for 2m radius air filled tunnel d=15 m deep in medium of constitutive parameters ϵ_r=4, σ=.001 mhos/m.

C. Tunnels with a Conducting Wire

Figures 12 and 13 show $E_{||}$ (or E^S/E^I) for a tunnel containing a circular wire located at the bottom and top respectively. The curves were computed using a one term moment method solution to represent the current on the wire, and the solution is cast in the form of the cylindrical Green's functions so that the boundary conditions at the surface of the cylinder can be easily satisfied. Figure 12 includes, for comparison, the normalized scattered field for the tunnel without the wire, and it is seen that the conducting wire is the dominant scatterer at low frequencies (the improvement in the example shown being 70 dB at 10 KHz). This is an important result because it means that a tunnel containing a wire (which may represent a power cable or a railway line) would be readily detectable using an LFW radar.

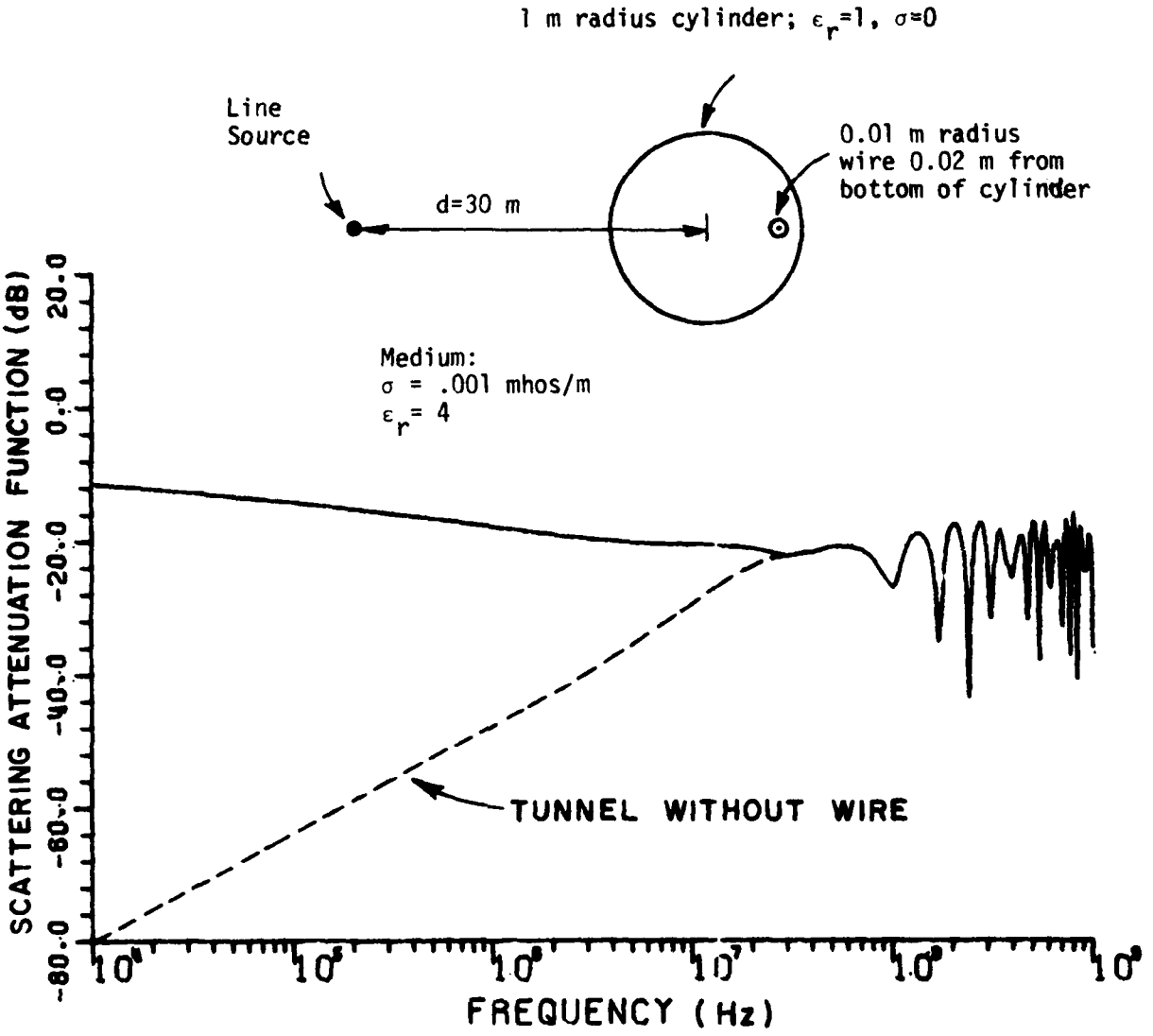

Figure 12. Scattering attenuation function for air filled cylinder with a perfectly conducting wire at the tunnel floor.

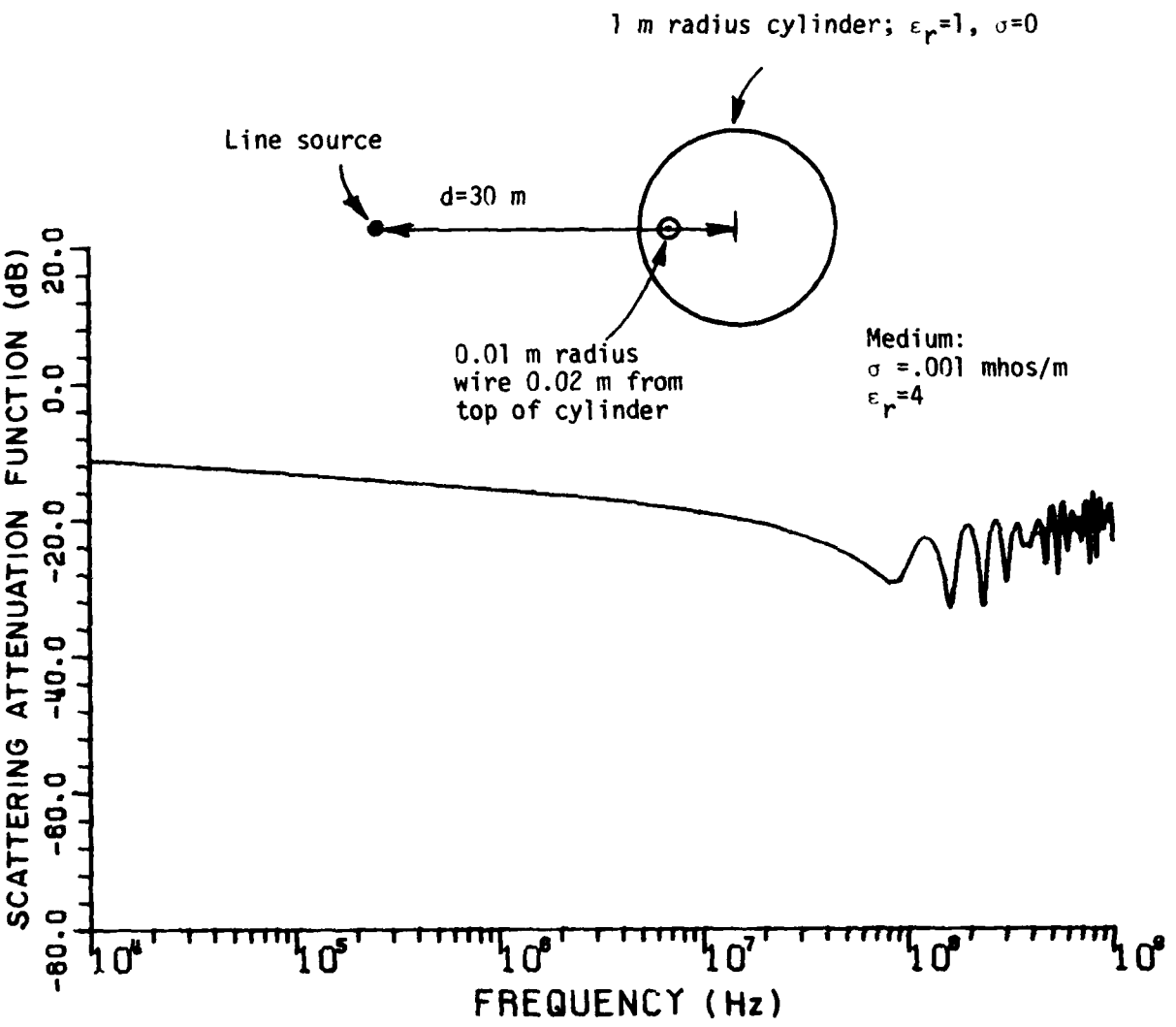

Figure 13. Scattering attenuation function for air filled cylinder with a perfectly conducting wire at the roof of the tunnel.

In the resonant region the normalized scattered fields are dominated by the tunnel resonances. In Figure 12 it it observed that the presence of the wire at the tunnel floor does not alter the scattering in the resonant region. This occurs because the illuminating rays diverge due to refraction as they enter the tunnel through the roof, and reflection occurs over a wide area of the tunnel floor which makes the wire almost "invisible". However when the wire is at the top of the tunnel it is in the relatively small area where the rays enter the tunnel and thus is very "visible". Figures 12 and 13 show that the presence of the wire at the tunnel roof decreases the level of the curve, but does not significantly alter the resonances.

Throughout this report, we focus attention on infinite cylinders and use these analyses as a basis for introducing the finite source. If the tunnel is finite in length the result is true for the specular reflection. In the case of the tunnel containing a wire, reflections of waves propagating within the tunnel from the ends of the tunnel can affect greatly the received signal. This is discussed in detail in Appendix II.

D. Square Tunnels

Figure 14 shows the normalized scattered fields for a square tunnel obtained using the hybrid moment method-eigenfunction technique [12]. Comparison with the results for a circular cylinder of similar size (Figure 10) shows that in the resonance region a square cylinder scatters 8 dB more strongly than an inscribed circular cylinder. This is due to the stronger reflection from the flat roof of the tunnel as compared to the rounded roof of the circular tunnel. At low frequencies the square tunnel scatters in the same way as does a circular tunnel, and in this case the square tunnel acts as a circular tunnel with an effective radius somewhere between 1 m and 2 m.

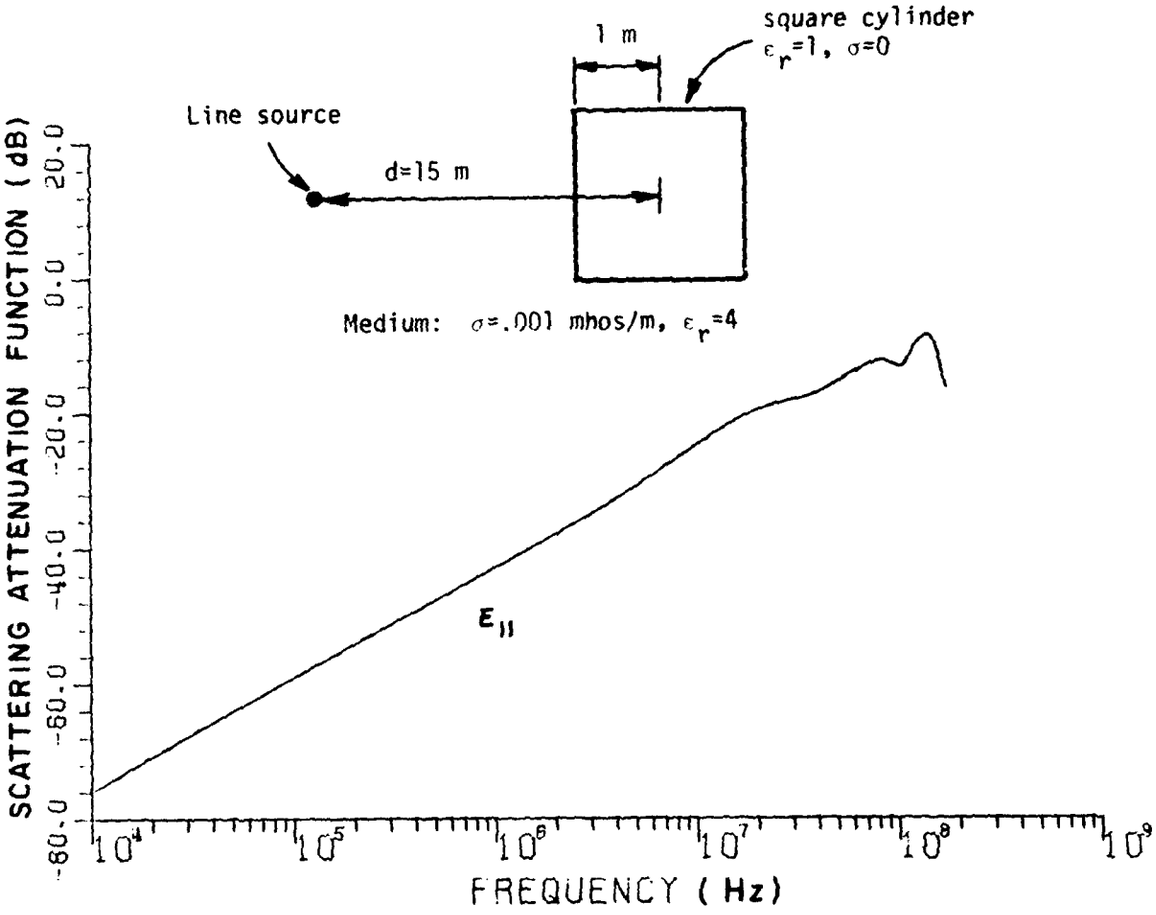

Figure 14. Scattering attenuation function for square air filled tunnel with side half length of 2m ootained by hybrid moment method-model solution.

IV. SYSTEM PROPERTIES

The goal of this report is to include scattered fields from targets other than the planar interface in the analysis of the response of a Video Pulse radar system. In the previous section we obtained the SAF for several cylindrical targets. In the following section we use that data to obtain the video pulse response for a tunnel.

A. Signals Received from Tunnels

The effect of the various features of the scattered fields of the tunnels on typical received radar signals is illustrated with some examples. Figure 15 shows the system responses for a 1 m long dipole 30 m from and parallel to, a 1 m radius infinite circular tunnel. The dipole has a 0.0015 m radius coating of polythene (ε_r=2.3). The upper plots are the reflection coefficient as a function of frequency $\rho(f)$ and the transmission coefficient $H(f)$ [9]. The lower plots show the signal reflected from the terminals of the antenna due to the input pulse and the signal received due to scattering from the cylinder. Because only one antenna is being modelled, the signal appearing at the antenna terminals is the sum of the two time plots. They are able to be shown separately for convenience because of the way the model is constructed (Figure 4). The time scales show that the two signals presented are separated by a clear range window. The transmitted signal was an 8 ns doublet, shown in Figure 16, and the parameters of this radar, which operates in the HFW, were chosen for strong illumination of the tunnel in the resonant region [9]. The tunnel resonances are clearly observed in the plot of $H(f)$ where it is seen that the first two resonances and the first antiresonance fall within the passband of the simple antenna system used. A wider passband is expected from improved antenna designs. The tunnel resonances cause a ripple with an 8 ns period on the tail of the received signal (for comparison Figure 17 shows the system responses when the target is a perfectly reflecting image plane, i.e., the SAF for the tunnel has not been included), and this kind of signature is suitable as input to an identification scheme based on the complex natural resonances of the cylinder [14]. If a wire were placed at the floor of the tunnel there would be no change in the received signal because the normalized scattered fields in the resonance region are unaffected by the presence of the wire. Figure 18 shows the system responses when the wire is placed at the roof of the tunnel. The ripple period remains at 8 ns, which is characteristic of the size of the tunnel. Figure 19 shows the system responses from a tunnel containing a wire buried 150 m deep. This signal was obtained using an LFW radar design with 50 m long dipoles and an 100 μs gaussian input pulse [9]. Without the wire this tunnel would not be detectable by an electromagnetic means.

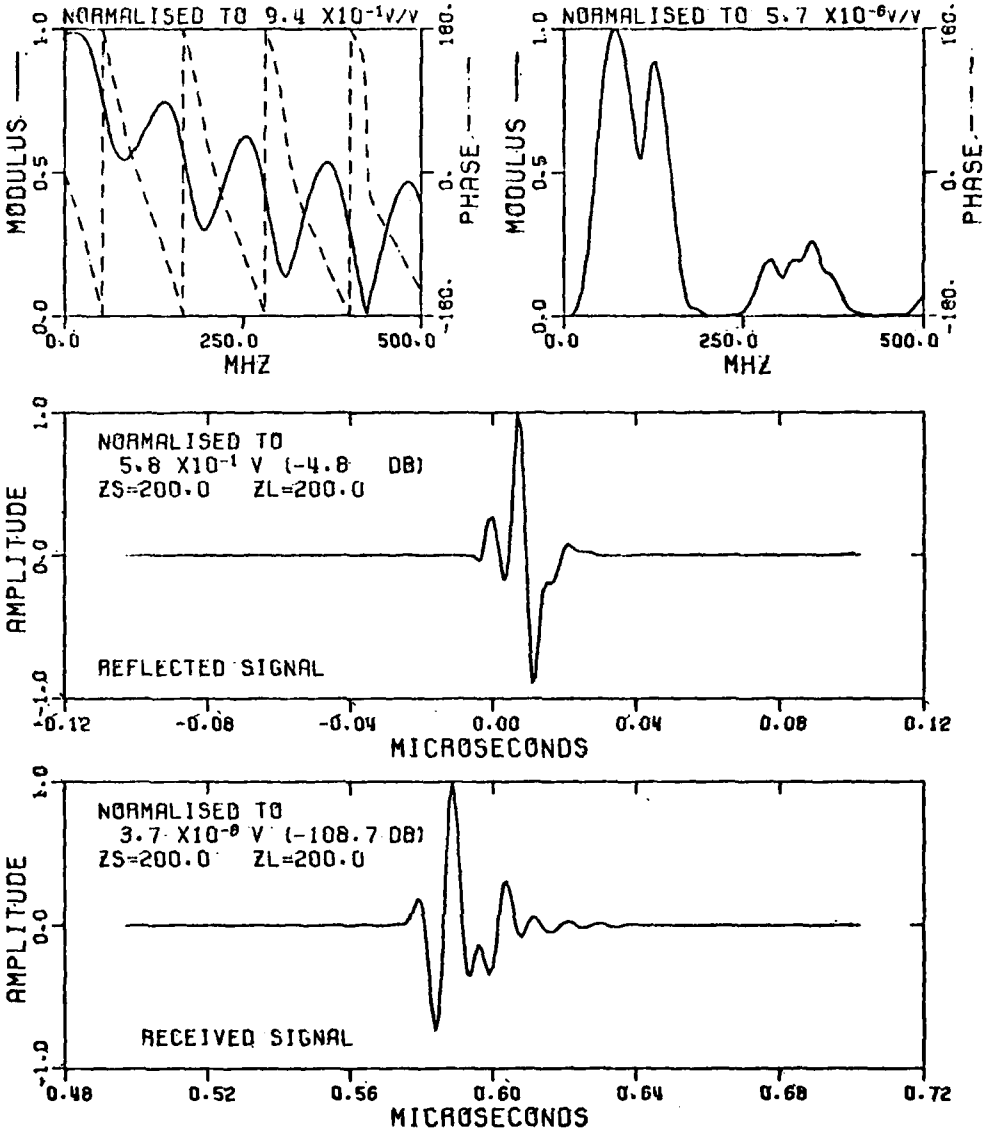

Figure 15. System responses for 1 m long dipole antenna parallel to and 30 m from 1 m radius circular air-filled tunnel in ground of constitutive parameters σ=.001 mhos/m and ε_r=9. The input pulse is an 8 ns gaussian doublet and the antenna load impedance is 200 ohms. The dipole is coated with a 0.0015 m radius layer of polythene insulation (ε_r=2.3). The meaning of the plots is given in the text.

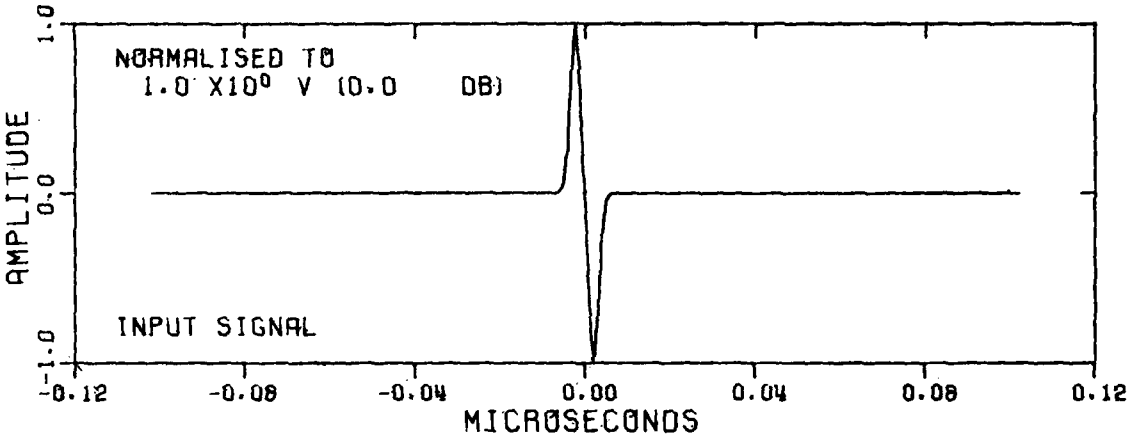

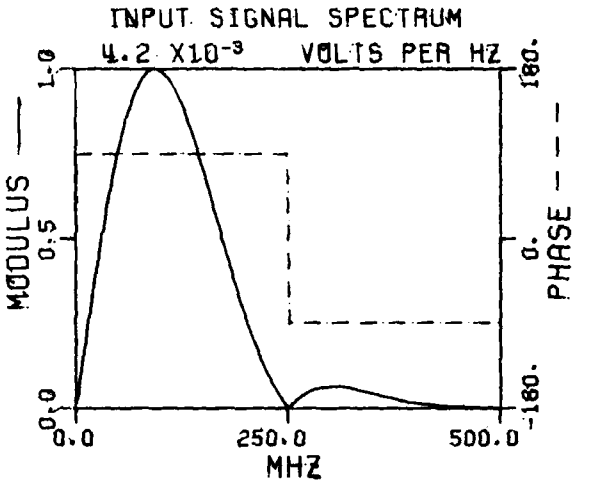

Figure 16. 8 ns gaussian doublet input signal (t_p= 4 ns).

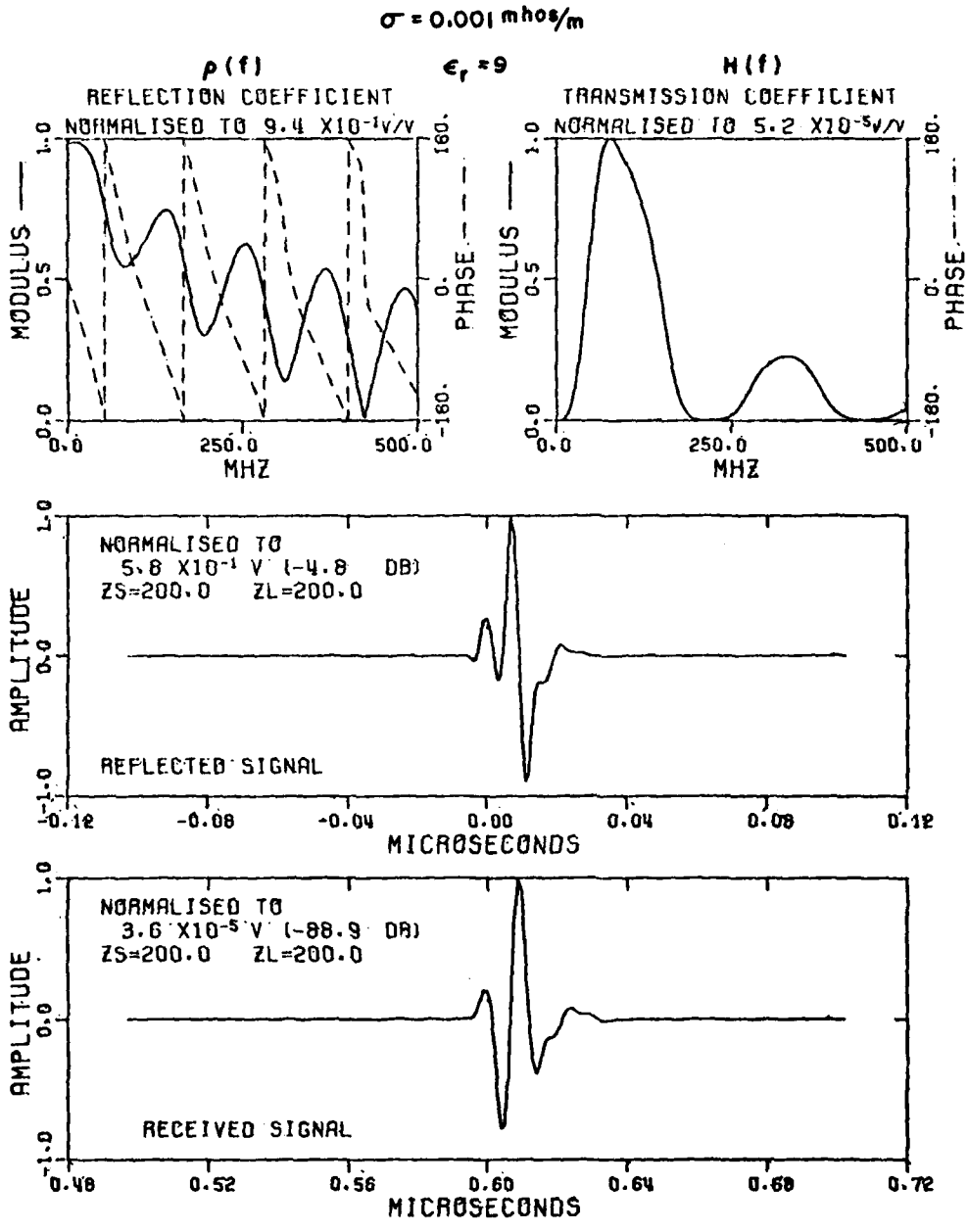

Figure 17. System responses for 1 m parallel dipoles spaced 60 m in ground of conductivity σ=0.001 mhos/m, ϵ_r=9. The system parameters are the same as for Figure 15 except that the SAF for the tunnel has not been included.

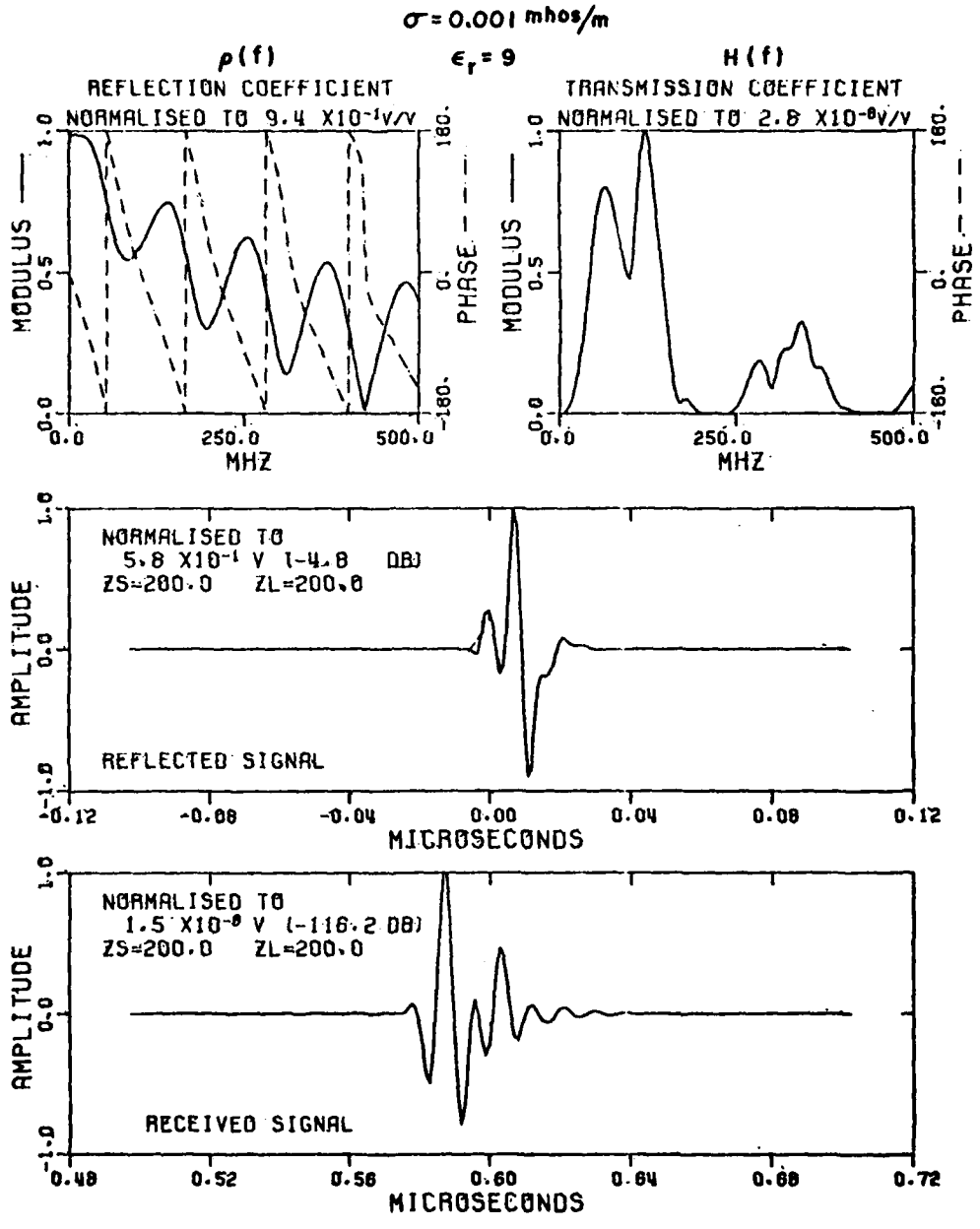

Figure 18. System responses for 1 m long dipole antenna parallel to and 30 m from a 1 m radius circular tunnel with a 0.01 m radius wire 0.02 m from the roof of the tunnel. The other system parameters are the same as for Figure 15.

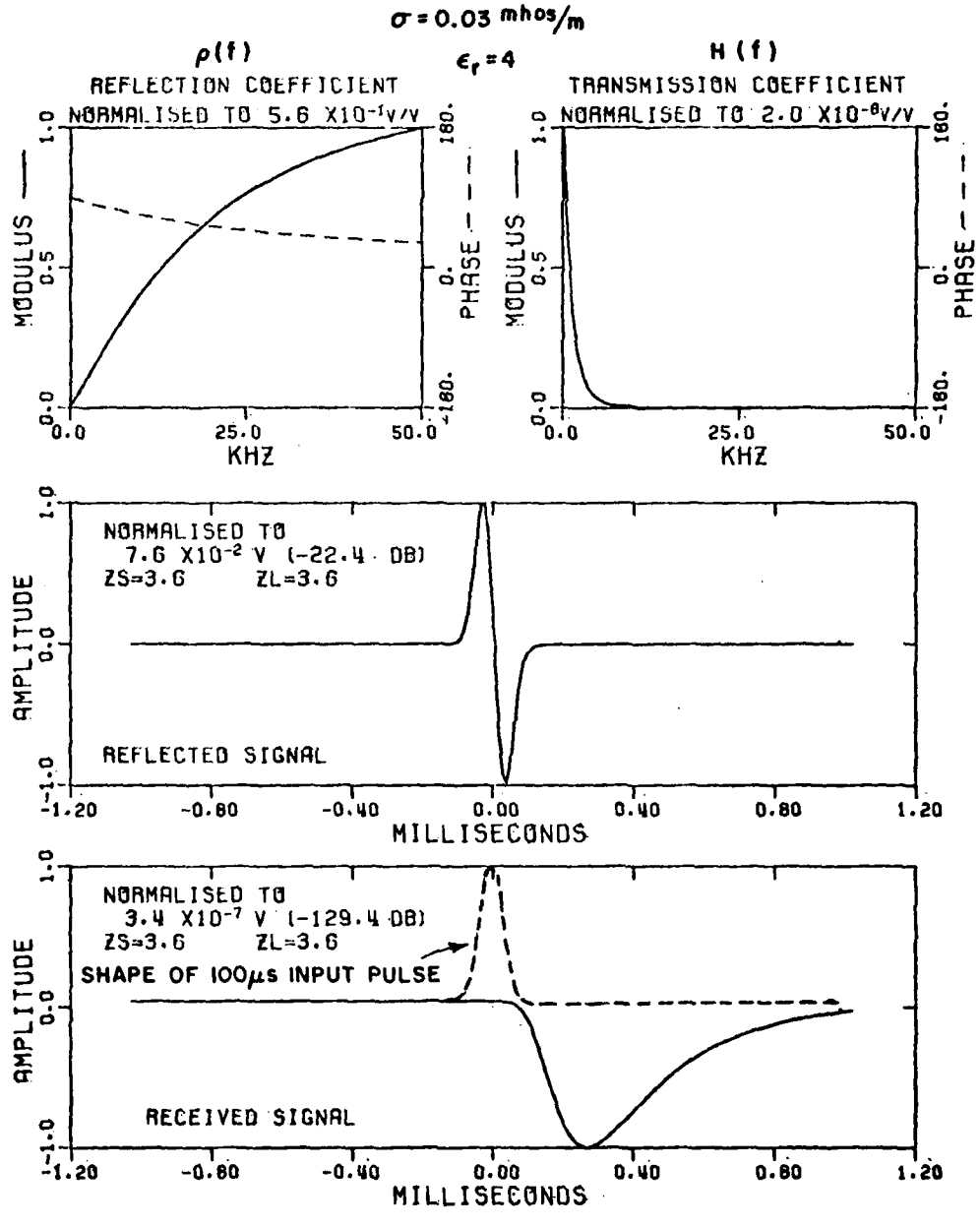

Figure 19. System responses for 50 m uninsulated dipole parallel to and 150 m from 1 m radius infinite tunnel containing a 0.01 m radius conducting wire 0.02 m from tunnel roof. The input signal was a 100 μs gaussian pulse.

Also shown in Figures 15-19 are several additional sets of data. The transmission and reflection coefficient is in reality the impulse response of the radar system (up to 500 MHz). It gives the received voltage as a function of frequency when excited by V_T = 1 volt at each frequency. Each curve in these figures is normalized by the value given. In Figure 16 the reflected signal is the reflected voltage waveform that would be reflected on a Z_S = 200 ohm feed cable when excited by the 8 ns Gaussian doublet. Figure 19 also illustrates the basic design concept developed in previous reports: that by careful design, the received pulse appears just after the duration of the transmitted pulse. Thus, in addition to the isolation achieved by the crossed dipole geometry there is further isolation introduced by the decay of the transmitted pulse before the received pulse appears.

B. Direct Mode Operation

A crossed dipole antenna system, with one dipole used for transmit and the other for receive, can provide about 100 dB of isolation between the transmitted and received signals. However only targets which couple energy from one dipole to the other can be observed (e.g., a parallel interface cannot be observed). However if the same dipole is used both for transmitting and receiving (called a direct mode system) then targets in which the scattered signal is polarized in the same sense as the incident signal can be observed. The direct mode system is practical if there is a large time separation between the transmitted signal and the received signal (called a clear range window). From Figure 15, it is observed that the received pulse is delayed by approximately 70 transmitted pulse widths. Clearly a pulser could be designed so that the transmitted pulse would decay well below the received pulse level when it arrives back at the antenna.

Second it may also be necessary to use the direct mode to detect planar interfaces and other targets that do not exhibit the desired polarization characteristics.

Figure 6 reveals that at frequencies such that the scattered field from the tunnel is above the fourth resonance, the scattered fields become independent of polarization. This means that the orthogonal mode geometry would not observe the tunnel when it is placed directly over the tunnel. In this case, it would be necessary to either use the direct mode system or to displace the antenna from the position directly above the tunnel. This latter concept is easily illustrated if the tunnel is placed in the plane of the crossed dipole pair as shown in Figure 20. Here the electric field incident (E^i) on the cylinder is now parallel to the cylinder. The scattered electric field E^s has a component parallel to receive dipole as shown. This applies to any target, for example, a spherical scatterer would produce no significant received signal if it is placed on the axis of symmetry of the cross dipole antenna symmetry. It would be observed however if it is displaced from this axis in planes not containing either antenna.

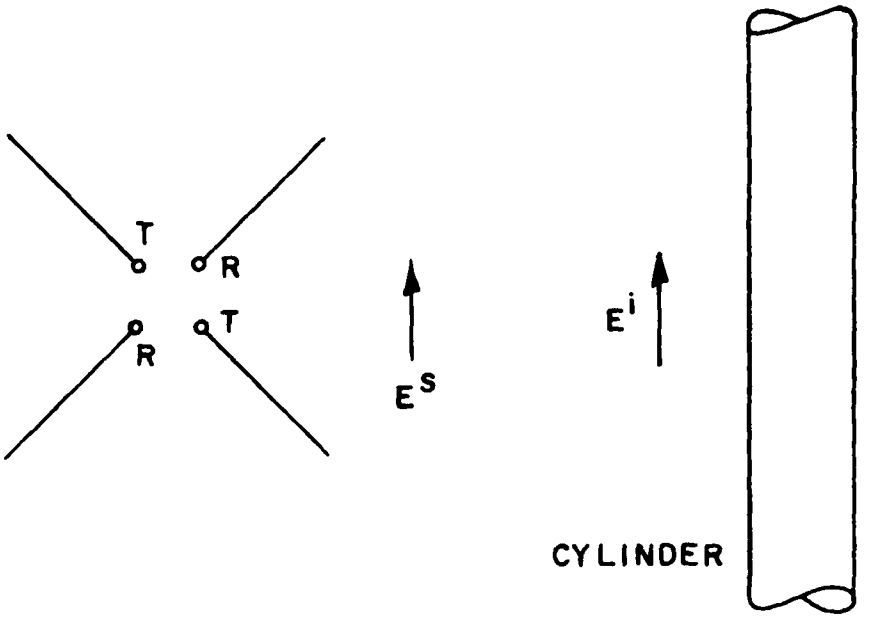

Figure 20. Illustrating the incident E^i and the scattered field E^S when the cylinder is in the plane containing the orthogonal dipole antenna system.

C. Influence of the Polarization Properties of the Target on the Received Signal

In order to better visualize the various situations that can occur for this radar system using the crossed dipole concept for isolation, let us represent the radiated field as being that caused by a z oriented dipole at the origin of the conventional spherical coordinate system. The radiated field is

$$\bar{E}_d = \hat{e}_\theta \, K \frac{e^{-jkr}}{r} \sin\theta \tag{12}$$

The voltage obtained on the receive crossed dipole are represented by those of an x oriented dipole at the position $(2r,\theta,\phi)$. If the reflection process does not alter the polarization of the wave then the received voltage is proportional to $\bar{E}_d \cdot \hat{e}_x$ where

$$\hat{e}_x = \hat{e}_\theta \cos\theta \cos\phi \tag{13}$$

or

$$V_r \propto \frac{e^{-jk2r}}{2r} \frac{1}{2} \sin 2\theta \cos \phi \tag{14}$$

In this case, the target would be any geometry that can be represented by a non-depolarizing scattering center or flare spot located at the position (r,θ,ϕ). If on the other hand, the target is polarization sensitive as is the case for a thin wire or thin cylinder then the wave incident on the target must be decomposed into its appropriate components.

For example, assume the scatterer to be a thin conducting cylinder. Such a target is an effective scatterer for waves polarized parallel to the cylinder. Thus the incident wave should be decomposed into two waves whose electric field is given by

$$\bar{E}_{inc} = \hat{e}_{\parallel} E_{\parallel} + \hat{e}_{\perp} E_{\perp} \tag{15}$$

Now the thin conducting cylinder is placed so that

$$y = d, \quad \text{and} \quad x = z \tan \theta' \tag{16}$$

where θ' is the angle between the cylinder and the x axis. The field scattered by the cylinder is now proportional to $\cos \theta'$, and the received voltage at the x oriented dipole at the origin

$$V_r'' \propto \frac{1}{2} \sin 2\theta'. \tag{17}$$

Similarly if the target scatters only the component of the wave polarized perpendicular to the cylinder,

$$V_r^{\perp} \propto -\frac{1}{2} \sin 2\theta' \tag{18}$$

where the negative sign indicates a reversal of polarity in comparison to that for parallel polarization.

There is also the possibility that the scattering caused by the two components of the incident wave satisfies neither of the above conditions i.e., neither scattering component vanishes. This was the case for the tunnels for frequencies up through the first few resonances. We define a complex proportionality constant

$$a_{\perp} = \frac{E_{\perp}^s}{E_{\parallel}^s} \tag{19}$$

where $E_{\parallel}^{s}$, $E_{\perp}^{s}$ are the scattered fields for the cylinder for incident polarizations parallel and perpendicular to the cylinder respectively.

Now Equation (15) may be written as

$$\bar{E}_{inc} = \hat{e}_{\parallel} E_d \cos \theta' + \hat{e}_{\perp} E_d \sin \theta' \qquad (20)$$

The received voltage is now

$$V_R' \propto \frac{1}{2} E_d \sin 2\theta' - \frac{1}{2} E_d a_{\perp} \sin 2\theta' \qquad (21)$$

$$\propto \frac{1}{2} E_d \sin 2\theta' (1 - a_{\perp})$$

For $a_{\perp} = 1$, $V_R' = 0$ corresponding to the case where the reflected field is orthogonal to the receiving dipole and is parallel to the transmitting dipole.

V. CONCLUDING REMARKS

Various cylindrical scattering models have been used to outline the expected performance of video pulse radar systems for the detection of cylindrical geometries. When incorporated with previous results for transmission between dipole antennas immersed in conducting media, these results provide the necessary design information for video pulse radars to detect tunnels.

APPENDIX I

DISCUSSION OF POTENTIAL ERRORS IN THE MODEL OF FIGURE 4

The reflecting plane of Figure 4 is positioned at the axis of the cylinder and yet it has been noted that for large hollow cylinders, the dominant scattering occurs at the front interface (or top of the tunnel). This Appendix shows that this reflector position does not modify the results.

First, it is observed that it makes no difference where the reflecting plane is placed in so far as the model of Figure 4a is concerned. However, it will influence both the model of Figure 4b (for the normalization E^I) and the separation of the dipole and its image shown in Figure 4c. Recall that the model of Figure 4c was introduced to treat the finite source and also to treat the influence of the ray divergence on the received voltage both in the plane of and perpendicular to the plane of the paper. If it is assumed that reflection occurs from the front interface as indeed appears reasonable, then our reflecting plane should be placed at that position. The major mechanism that could contribute to errors would be the loss introduced by the media. It could be argued that the energy enters the tunnel at the top and the tunnel (being free space) is loss-less. We are concerned with the changes introduced in both the models of Figure 4b and 4c when the reflecting plane is so moved. The ray divergence in the plane of the paper of Figure 4c can be represented by a line source perpendicular to the paper. The fields of that line source are given by

$$U = U_o\, e^{-\gamma\rho_1} \sqrt{\frac{\rho_1}{\rho_1 + r}}\; e^{-\gamma r} \tag{A1}$$

where the factor $U_o e^{\gamma\rho_1}$ equals the fields incident of the ground plane at a distance $\rho_1 = d$, the factor

$$\sqrt{\frac{\rho_1}{\rho_1 + r}} = \sqrt{\frac{d}{d + r}} \tag{A2}$$

is the spatial divergence factor and represents the decay in the fields caused by ray spreading as the observation distance r moves away from the source point, the factor $e^{-\gamma r}$ represents the usual phase delay factor plus the attenuation introduced by the medium. The fields scattered by a plane at the axis of the cylinder is represented by $r = d$ whereas the fields scattered by a plane at the front interface is represented by $r = d - 2a$. Thus the factor

$$\frac{U(d-2a)}{U(d)} = e^{2\gamma a}\sqrt{\frac{d}{d-a}} \qquad \text{(A3)}$$

represents the error introduced in the model of Figure 4c.

The factor E^I would increase by $e^{2\gamma a}$ if the reference plane is shifted to the top of the tunnel. This cancels the factor $e^{-2\gamma a}$ in Equation (A-3). The resulting error in Equations (10) and (11) is then only

$$\sqrt{\frac{d}{d-a}} \qquad \text{(A4)}$$

This result implies that the reference plane can be taken at any convenient position as long as it is consistent with both the models of Figures 4(b) and 4(c), and the amplitude of the result so obtained is modified by the $\sqrt{d/d-a}$ factor. This was confirmed by recomputing the result of Figure 15 with the reference plane moved to a point one half of the distance from the target to the source. The result was exact in shape and differed by 3 dB in amplitude.

An important advantage of this result is that for an HFW radar the results for tunnels buried at different depths can be computed from one frequency response calculation for the model of Figure 4(c).

APPENDIX II

DETECTION OF FINITE LENGTH TUNNELS CONTAINING CONDUCTING WIRES

Throughout this report, we have focussed attention on infinite cylinders and have used these analyses as a basis for introducing the finite source. The question naturally arises concerning the required length of the cylinder in order that this analysis correctly predict the detectability of the tunnel.

We have considered two basic types of cylinder, the dielectric cylinder or tunnel, and the conducting cylinder. The conducting cylinder was observed to give a very high scattered field whether or not the conductor was in electrical contact with the ground. If the conducting cylinder is in electrical contact with the conducting ground the high scattered fields are obtained since the currents can flow into and be attenuated by the medium and are not required to vanish at the end of the cylinder. This was seen earlier in Figure 5.

The required length becomes much greater if the conducting wire is insulated since it now becomes the center conductor of a coaxial quasi-TEM mode* transmission line. The loss can be estimated from the case of propagation of a TM wave over a lossy earth [15]. This propagation loss is in general much lower than that corresponding to propagation in the medium since most of the energy propagates in the free space region of the tunnel and not in the conducting medium. Consequently if we depend on absorption to cause the fields to decay to a low value by the time they reach the end of a wire, a very long tunnel is required. For example at one KHz, satisfactory absorption has not been achieved even if the wire is 6,400 m long for $\sigma = 10^{-3}$ mhos/m, which means that the the infinite cylinder model is inadequate for modelling tunnels containing insulated donducting wires. It also implies that in order to detect such a geometry using a c.w. system the frequency must be carefully selected to correspond to a tunnel resonance. This resonance is discussed later. A properly designed video pulse radar will illuminate the target in its resonant region. This is in direct contrast to the case where the wire is in electrical contact with the conducting earth as was shown in Figure 5 for a 1000 m long wire. (The presence of the tunnel near the wire is not expected to significantly alter the results.)

For a pulsed system observing the insulated wire is all that is required. Since propagation of waves in the tunnel occurs with very much less loss than propagation through the conducting medium, the strongest signals from the ends of the tunnel will be observed for the down along and return path illustrated in Figure 21. The propagation velocity of the quasi-TEM

*It is actually a TM mode since there is now a slight longitudinal component of the electric field.

wave in the tunnel can also be estimated [15] and it turns out that it is comparable to the speed of light.

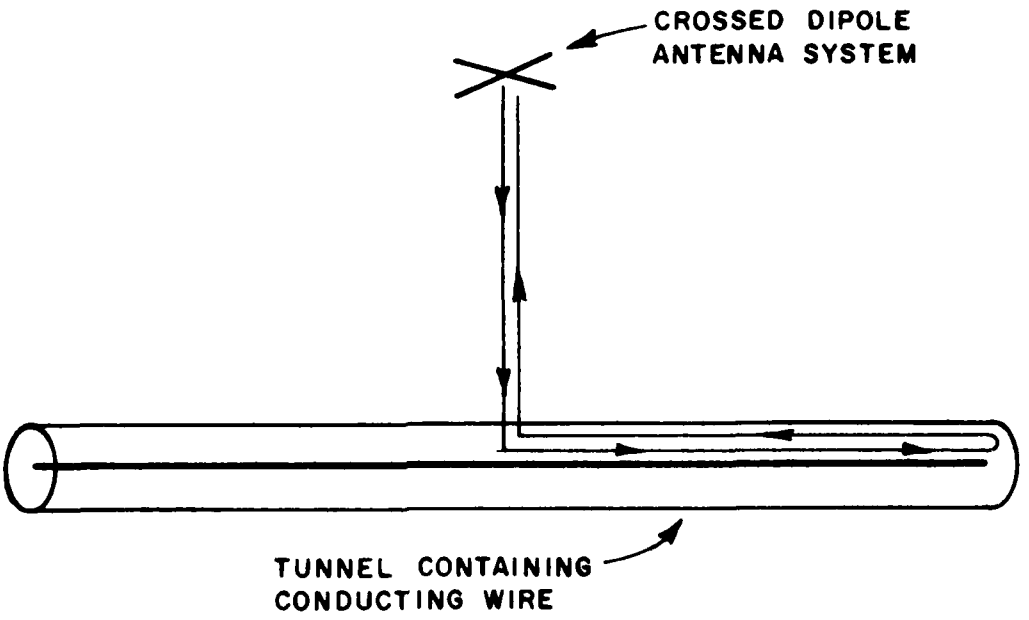

Figure 21. Illustrating down, along and return propagation path for buried tunnel containing wire.

Consider the signal shown in Figure 22. This signal is received on a 50 m long dipole parallel to, and 50 m away from a 0.1 m radius infinite tunnel ($\varepsilon_r = 1$) containing a 0.01 m radius conducting wire at its center. The input pulse was 0.5 μs gaussian. If a crossed dipole antenna system was used, then the signal would have had an amplitude of -104 dB. Let us assume a design criterion that the tunnel is detectable if end reflections arrive after the received signal has reached peak magnitude. Thus the length of the tunnel should exceed the length equivalent to a return propagation time of 1 μs, which (at the speed of light) is $\pm$ 150 m from the point vertically below the radar antenna. This represents a relatively short tunnel. Figure 23 shows the received signals obtained from a complete moment method solution for a 300 m long 0.1 m radius tunnel containing a 0.01 m radius wire at its center. In this complete solution a 50 m uninsulated orthogonal dipole antenna system was used so that the model is exact (with the exception of the interface which increases the received signal by about 6 dB [9]. Previous results in this report have been presented for parallel dipoles so that the result differs by 6 dB in

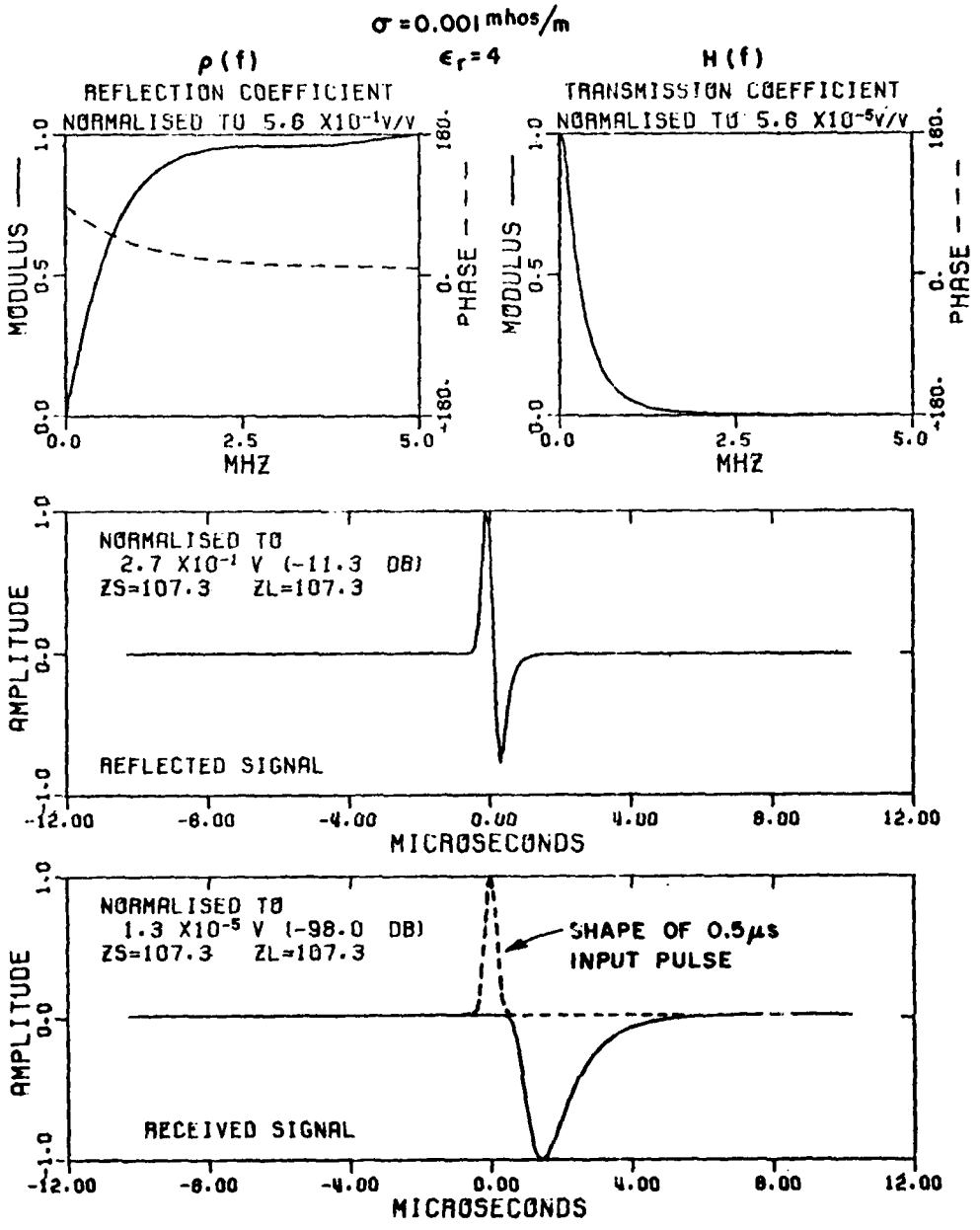

Figure 22. System responses for 50 m long uninsulated dipole antenna parallel to and 50 m away from 0.1 m radius infinite tunnel containing a 0.01 m radius perfectly conducting wire on its axis. The input signal was a 0.5 μs gaussian pulse.

amplitude (Equation (11)) if the scatterer is polarization dependent. Both the early time behavior and the complete received signal are shown in Figure 23(a) and (b). There is a prominent resonance at about 200 KHz (shown later) corresponding to the length of the tunnel and the received signal displays a ringing characteristic of this resonance. The significant feature of this signal is that it has a long duration, and is thus in a clear range window which makes it readily detectable. Observe also that the amplitude is 13.6 dB smaller than that for the infinite tunnel. For the finite tunnel the specular reflection is observed to be of shorter duration than that for the infinite tunnel. This indicates that the higher frequency components of the input signal are arriving sooner than the low frequency components. It is observed that the specular reflection is not necessary for detection of the tunnel: the tunnel is clearly detectable by its late time (resonant) behavior. The resonant frequency may be useful as a gauge of the tunnel length. Hence we can afford to increase the duration of the input signal to put more energy into the resonant band of the tunnel without sacrificing signal detectability. The effect of increasing the input pulse duration is shown in Figures 23(c)-(f). Detectability of the signal is enhanced because of the increased amplitude. This occurs because the highest frequency in the input signal spectrum is reduced which means that (a) the spectrum more closely corresponds to the LFW and (b) more energy is supplied at the tunnel resonant frequency.

These results suggest that the criterion proposed earlier is conservative. The signal received from 150 m, 75 m, and 37.5 m long tunnels are shown in Figure 24 for appropriate input signals which demonstrates that tunnels considerably shorter than the length predicted can be detected.

Figure 25 shows the magnitude of the transmission transfer function [9] for the orthogonal antenna system and the four finite tunnels analyzed here. For the 300 m tunnel (Figure 25(a)) the first resonance at 200 KHz, and the second resonance are clearly visible. As the tunnel becomes shorter, the resonant frequency increases, which increases the ringing frequency as observed in Figure 24. For the 37.5 m long tunnel, the resonant frequency lies above the LFW critical frequency. Thus the increased scatter at the tunnel resonant frequency is negated by the higher losses in the earth media. This produces a wide system bandwidth which results in the short duration received signal shown in Figure 24(c).

Figure 25 shows that for a cw radar system to detect long tunnels the operating frequency needs to be carefully chosen to correspond very closely to the longitudinal resonant frequency of the tunnel. Without knowledge of the tunnel length this is difficult to predict. However a video pulse radar can, in one measurement, illuminate the tunnel with a wide band of frequencies.

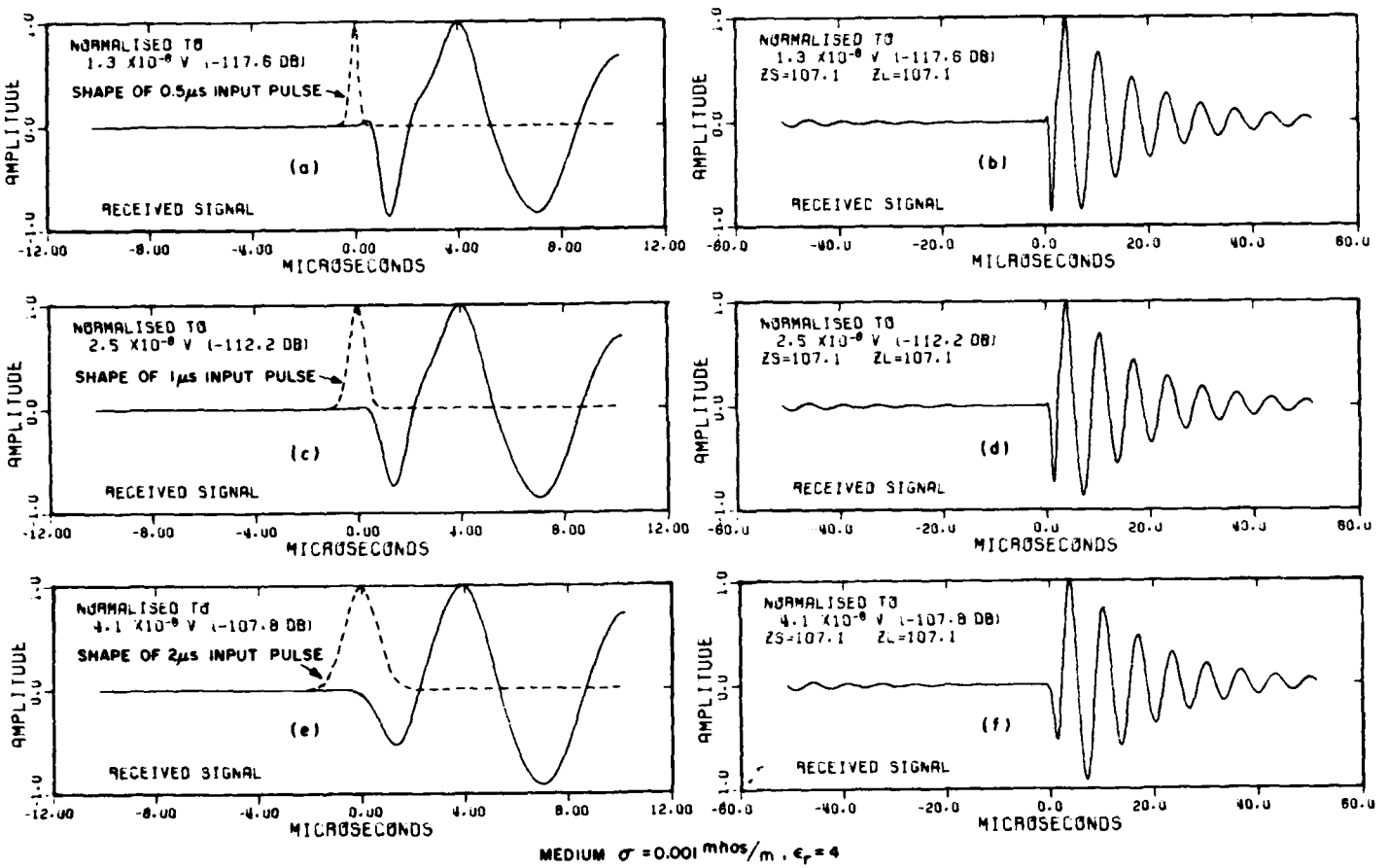

Figure 23. Signals received on 50 m orthogonal dipole antenna system 50 m from a 300 m long, 0.1 m radius. Tunnel containing a 0.01 m radius wire on its axis. (a) and (b) show the early time behavior and the complete received signal respectively for a 0.5 μs gaussian input pulse. (c) and (d), and (e) and (f) show the signals for 1 μs and 2 μs input pulses respectively.

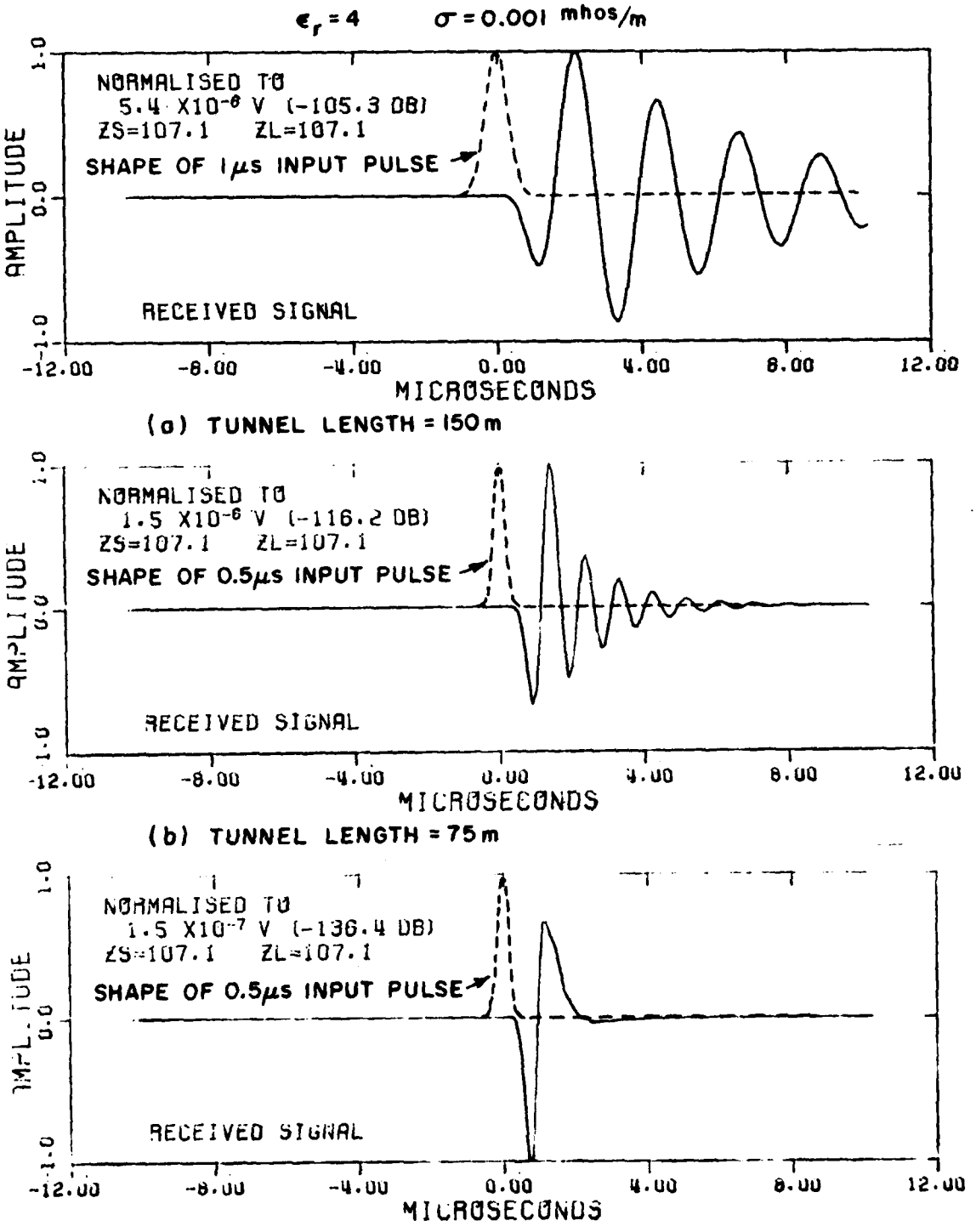

Figure 24. Signals received on receive dipole of 50 m orthogonal dipole antenna system 50 m from a finite length tunnel for various tunnel lengths. The tunnel is 0.1 m radius and contains a 0.01 m radius wire at its center.

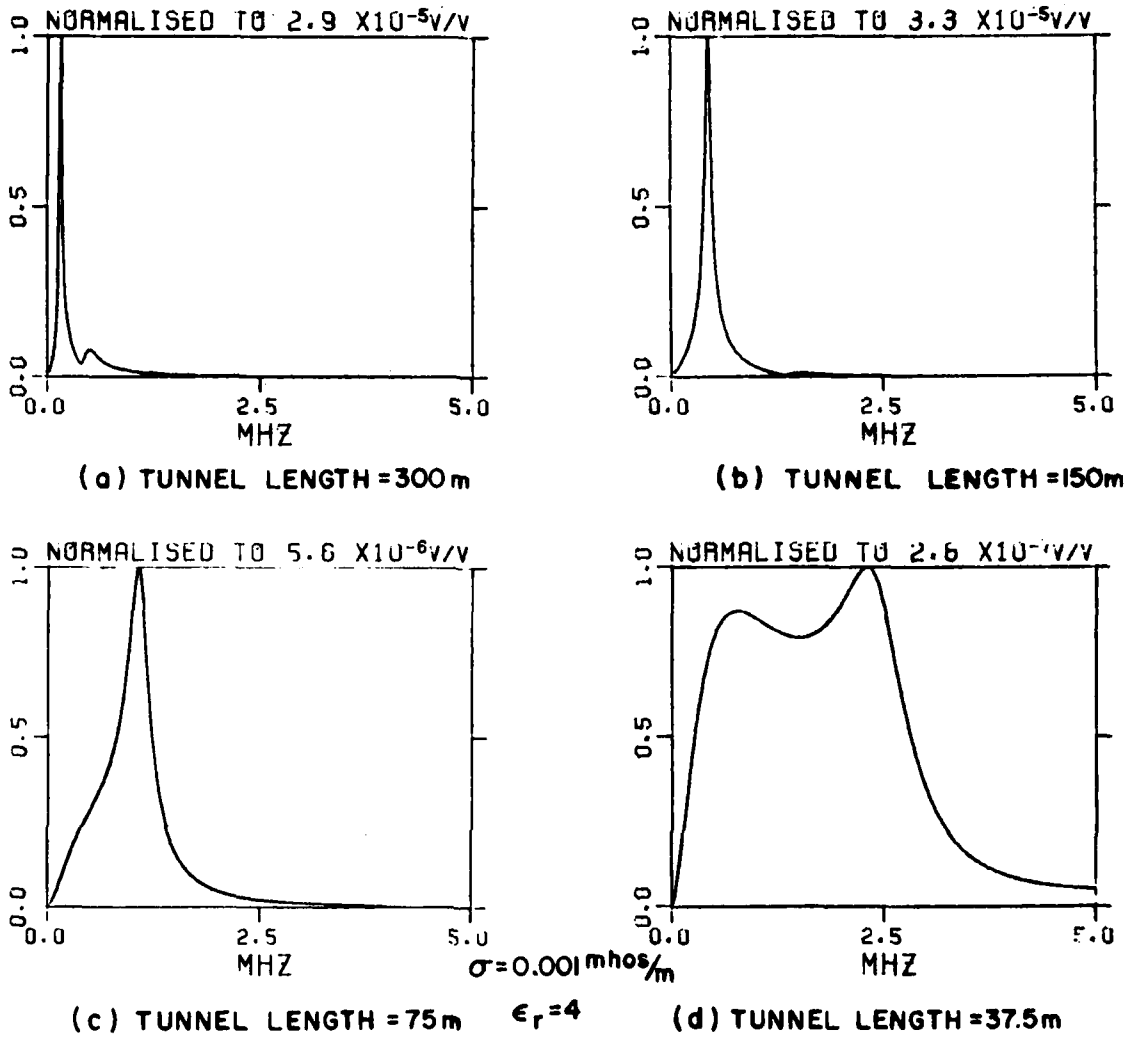

Figure 25. Magnitude of transmission transfer function for 50 m long, 0.002 m radius uninsulated dipole antenna system 50 m in from a finite length tunnel for various tunnel lengths. The tunnel is 0.1 m radius and contains a 0.01 m radius wire at its center.

It is noted that the results presented in this Appendix are for tunnels which are open-circuited, i.e., the conducting wire is not connected to the ground at the end of the tunnel. If, for example the wire was grounded at the tunnel entrance, as is possible with electric cables, then the sign of the reflection coefficient at the end of the tunnels is changed and there would be a consequent change in the scattered signal.

REFERENCES

[1] J. D. Young and R. Caldecott, "Underground Pipe Detector," U. S. Patent 3,967,282, June 29, 1976.

[2] J. D. Young, "A Transient Underground Radar for Buried Pipe Location," USNC/URSI Meeting, Boulder, Colorado, October 23, 1975.

[3] A. C. Eberle and J. D. Young, "Development and Field Testing of a New Locator for Buried Plastic and Metallic Utility Lines," presented at 56th Annual meeting of the Transportation Research Board, Washington, D.C., January 24-28, 1977.

[4] D. L. Moffatt and L. Peters, Jr., "An Electromagnetic Pulse Hazard Detection System," Proc. 1972 North American Rapid Excavation and Tunnelling Conference, Chapter 4, June 1972.

[5] D. L. Moffatt, R. J. Puskar and L. Peters, Jr., "Electromagnetic Pulse Sounding for Geological Surveying with Application in Rock Mechanics and the Rapid Excavation Program," Report 3408-2, The Ohio State University ElectroScience Laboratory, Department of Electrical Engineering; prepared under Contract H0230009 for Advanced Research Projects Agency, 1973.

[6] D. L. Moffatt and R. J. Puskar, "A Subsurface Electromagnetic Pulse Radar," Geophysics, vol. 41, pp. 506-518, June 1976.

[7] R. S. Vickers and L. T. Dolphin, "Subsurface Radar Sounding Experiments in Archaeology," USNC/URSI Meeting, Boulder, Colo., October 23, 1975.

[8] N. N. Wang, L. Ersoy, and W. D. Burnside, "GTD Analysis and the Hybrid Techniques for the Investigation of the Surface Current and Charge Densities Induced on Aircraft," Report 4172-1, December 1976, The Ohio State University ElectroScience Laboratory, Department of Electrical Engineering; prepared under Contract F29601-75-C-0086 for Kirtland Air Force Base, New Mexico.

[9] G. A. Burrell, L. Peters, Jr. and A. J. Terzuoli, Jr., "The Propagation of Electromagnetic Video Pulses with Application to Subsurface Radar for Tunnel Detection," Report 4460-2, December 1976, The Ohio State University ElectroScience Laboratory, Department of Electrical Engineering; prepared under Contract DAAG53-76-C-0179 for U. S. Army Mobility Equipment Research and Development Command.

[10] R. G. Kouyoumjian, L. Peters, Jr., and D. T. Thomas, "A Modified Geometrical Optics Method for Scattering by Dielectric Bodies," IEEE Trans., Vol. AP-11, 1963, pp. 690-703.

[11] L. Peters, Jr., T. Kawano and W. G. Swarner, "Approximations for Dielectric or Plasma Scatterers," Proc. IEEE, vol. 53, 1965, pp. 882-892.

[12] J. H. Richmond, H. B. Tran, Report 4460-4 (in preparation).

[13] J. H. Richmond, "Radiation and Scattering by Thin-Wire Structures in a Homogeneous Conducting Medium," IEEE Trans., Vol. AP-22, p. 365, March 1974.

[14] C. W. Chuang and D. L. Moffatt, "Natural Resonances of Radar Targets via Prony's Method and Target Discrimination," IEEE Transactions on Aerospace and Electronic Systems, Vol. AES-12, n. 5, September 1976, pp. 583-589.

[15] S. Ramo and J. R. Whinnery, Fields and Waves in Modern Radio, New York, John Wiley, 1944.